

1 **A post-assembly conformational change makes the SARS-CoV-2 polymerase** 2 **elongation-competent**

3

4 Misha Klein^{1*}, Arnab Das^{1*}, Subhas C. Bera^{2*}, Thomas K. Anderson³, Dana Kocincova⁴, Hery W. Lee⁴,
5 Bing Wang⁵, Flavia S. Papini², John C. Marecki⁶, Jamie J. Arnold⁷, Craig E. Cameron⁷, Kevin D. Raney⁶,
6 Irina Artsimovitch⁵, Mathias Götte⁴, Robert N. Kirchdoerfer³, Martin Depken^{8,#}, David Dulin^{1,2,#}

7 1 Department of Physics and Astronomy, and LaserLaB Amsterdam, Vrije Universiteit Amsterdam,
8 De Boelelaan 1081, 1081 HV, Amsterdam, The Netherlands

9 2 Junior Research Group 2, Interdisciplinary Center for Clinical Research, Friedrich-Alexander-
10 University Erlangen-Nürnberg (FAU), Cauerstr. 3, 91058 Erlangen, Germany

11 3 Department of Biochemistry and Institute for Molecular Virology, University of Wisconsin-Madison,
12 Madison, WI 53706

13 4 Department of Medical Microbiology and Immunology, University of Alberta, Edmonton, Alberta
14 T6G 2R3, Canada

15 5 Department of Microbiology and The Center for RNA Biology, The Ohio State University, Columbus,
16 Ohio, USA

17 6 Department of Biochemistry and Molecular Biology, College of Medicine, University of Arkansas for
18 Medical Sciences, Little Rock, AR 72205 USA.

19 7 Department of Microbiology and Immunology, University of North Carolina School of Medicine,
20 Chapel Hill, NC 27599 USA

21 8 Department of Bionanoscience, Kavli Institute of Nanoscience, Delft University of Technology, Van
22 der Maasweg 9, 2629 HZ Delft, The Netherlands

23

24 *These authors contributed equally to the present work.

25 #: To whom the correspondence may be addressed: d.dulin@vu.nl; s.m.depken@tudelft.nl

26 **Keywords**

27 SARS-CoV-2, RNA virus, polymerase, single-molecule biophysics, magnetic tweezers

28

29 **Abstract**

30 Coronaviruses (CoV) encode sixteen non-structural proteins (nsps), most of which form the replication-
31 transcription complex (RTC). The RTC contains a core composed of one nsp12 RNA-dependent RNA
32 polymerase (RdRp), two nsp8s and one nsp7. The core RTC recruits other nsps to synthesize all viral
33 RNAs within the infected cell. While essential for viral replication, the mechanism by which the core
34 RTC assembles into a processive polymerase remains poorly understood. We show that the core RTC
35 preferentially assembles by first having nsp12-polymerase bind to the RNA template, followed by the
36 subsequent association of nsp7 and nsp8. Once assembled on the RNA template, the core RTC
37 requires hundreds of seconds to undergo a conformational change that enables processive elongation.
38 In the absence of RNA, the (apo-)RTC requires several hours to adopt its elongation-competent
39 conformation. We propose that this obligatory activation step facilitates the recruitment of additional

1 nsp's essential for efficient viral RNA synthesis and may represent a promising target for therapeutic
2 interventions.
3

1 Introduction

2 The COVID-19 pandemic is caused by the severe acute respiratory syndrome coronavirus 2
3 (SARS-CoV-2) with devastating impacts on public health that are still ongoing (WHO:
4 <https://data.who.int/dashboards/covid19/cases?n=c>). Novel CoVs may also emerge in the future, as the
5 present pandemic comes close on the heels of the MERS-CoV in 2012 and SARS-CoV-1 in 2002. Viral
6 genome replication and transcription are important targets for therapeutic interventions due to their
7 conserved nature across CoVs, and treatments based on nucleotide analogs, such as remdesivir (1)
8 and molnupiravir (2), have proven to be effective. However, CoVs have a great ability to evolve and
9 adapt, either via mutation or recombination (3–5). Having a precise understanding of the molecular
10 determinants in CoV replication and transcription will help design future antiviral drugs to counter such
11 adaptation.

12
13 CoVs are positive (+)RNA viruses with a ~30 kb long single-stranded (ss) genome. The 5'-
14 proximal two thirds encode for the sixteen non-structural proteins (nsp(s)) (13). These nsps are encoded
15 on two open reading frames separated by a ribosomal frameshifting sequence within the nsp12-
16 polymerase gene. Translation produces two polyproteins: one spanning from nsp1 to nsp11, and the
17 other from nsp1 to nsp16. These polyproteins are subsequently processed into individual nsps by two
18 proteases—nsp3 (papain-like protease) and nsp5 (3C-like protease). Notably, nsp5 processes all nsps
19 from nsp4 to nsp16 (14). Most of the nsps associate to form the replication-transcription complex (RTC),
20 which synthesizes all viral RNAs in the infected cell (15, 16). The minimal complex capable of RNA
21 synthesis consists of the nsp12-polymerase associated with nsp7 and nsp8 in a 1:1:2 stoichiometry
22 (hereafter 'core RTC') (10, 17–20). Nsp7 and nsp8 are required for *in vitro* RNA primer-extension by
23 the core RTC (21–24).

24
25 Previous studies have shown that it takes several minutes for the CoV core RTC to perform
26 detectable primer-extension in *in vitro* bulk assays (23, 24). This is particularly striking, as the SARS-
27 CoV-2 core RTC is the fastest RNA polymerase reported to date, with a nucleotide addition rate up to
28 ~180 nt/s at 37°C (11). The apparent lag time in primer-extension assays therefore seems to stem from
29 a step prior to RNA synthesis and has been proposed to arise from a stepwise assembly of the individual
30 nsps into the core RTC (22, 23, 25). However, no quantitative assessment of different contributors to
31 the lag times has been reported to date. Characterizing the mechanism through which nsp7 and nsp8
32 regulate primer-extension by the core RTC requires a more in-depth comparison of their influence, both
33 before (hereafter 'activation phase') and during (hereafter 'elongation phase') RNA synthesis (**Figure**
34 **1A**).

35
36 We set out to understand the path the CoV core RTC proteins take towards polymerase activity
37 by using a high-throughput single-molecule magnetic tweezers assay (26) in conjunction with kinetic
38 modelling. Previously, we used the same assay to study the elongation phase of the SARS-CoV-2 core
39 RTC in-depth (26). Here, we used our ability to detect the onset of elongation from individual RNA
40 primer-templates to differentiate between the time spent by single core RTCs on activation and

1 elongation. Our data and kinetic model reveal that a core RTC is not in an elongation-competent
2 conformer upon assembly. As such, the core RTC must undergo a conformational change that allows
3 it to enter the elongation phase. We start by confirming that a core RTC (reconstituted from individually
4 expressed proteins) exhibits a considerable lag-time prior to elongation (23, 24). The lag time does not
5 stem from the time required to assemble the complex since activation times remain substantial at
6 saturating protein concentrations. Instead, nsp7, nsp8, and the template RNA appear to greatly limit the
7 conformational space to be explored by the core RTC, allowing it to adopt its elongation-competent
8 conformer within minutes. The conformational change occurs prior to the elongation phase as factors
9 influencing the kinetics of the activation phase have no effect on the elongation phase. Finally, even in
10 the presence of nsp13-helicase an average activation time of several hundreds of seconds remains.
11 Our results reveal a mandatory step towards assembling a complete and functional CoV-RTC, opening
12 new avenues for antiviral drug development.

13

14 **Materials and Methods**

15 **Purification and recombinant protein expression of nsp7 and nsp8 from SARS-CoV-2.**

16 This protocol was described in detail in (6, 26). The SARS-CoV-2 nsp7 and nsp8 genes were
17 cloned into pET46 (Novagen) with an N-terminal 6 histidine tag and a TEV protease site for purification.
18 The proteins were recombinantly expressed in Rosetta2 pLys *E.coli* (Novagen) and purified using Ni-
19 NTA agarose beads. Nsp7 and nsp8 proteins were further purified by size exclusion chromatography.
20 Purified proteins were dialyzed into storage buffer (10 mM HEPES, pH 7.4, 300 mM NaCl, 2 mM DTT),
21 aliquoted, and stored at -80 °C.

22

23 **Purification and recombinant protein expression of nsp12-polymerase in Sf9 cells.**

24 This protocol was described in detail in (6, 26). The SARS-CoV-2 nsp12-polymerase gene was
25 cloned into pFastBac with a TEV site and strep tag (Genscript) for efficient purification. The bacmid was
26 created in DH10Bac *E.coli* (Life Technologies) and amplified in Sf9 cells (Expression Systems) with
27 Cellfectin II (Life Technologies) to generate recombinant baculovirus. Sf21 cells were infected, and the
28 cell lysate cleared by centrifugation and filtration. The protein was purified via strep tacin agarose and
29 further polished in size exclusion chromatography. Purified protein was dialyzed into storage buffer (10
30 mM HEPES, pH 7.4, 300 mM NaCl, 0.1 mM MgCl₂, 2 mM TCEP), aliquoted, and stored at -80 °C.

31

32 **Purification and recombinant protein expression of nsp12-polymerase in *E. coli*.**

33 The protocol used to obtain nsp12-RdRp used for these experiments was described in detail in
34 (27). Nsp12-polymerase was overexpressed in *E. coli* BL21(DE3) cells (Novagen). The cleared lysate
35 was applied to Ni21-NTA resin (Cytiva) and the eluted protein was further purified by anion exchange
36 chromatography and size exclusion chromatography. Purified protein was dialyzed into storage buffer
37 (20 mM HEPES, pH 7.5, 150 mM KCl, 45% glycerol, 1 mM MgCl₂, 1 mM DTT), aliquoted, and stored
38 at -80 °C.

1

2 **Purification of co-translated SARS-CoV-2 core RTC.**

3 The protocol was described in detail in (12). The pFastBac-1 (Invitrogen, Burlington, ON,
4 Canada) plasmid with the codon-optimized synthetic DNA sequences (GenScript, Piscataway, NJ,
5 USA) coding for SARS-CoV-2 (NCBI: QHD43415.1) nsp5, nsp7, nsp8, and nsp12 were used as a
6 starting material for protein expression in insect cells (*Sf9*, Invitrogen, Waltham, MA, USA) (8, 9, 12,
7 28). We employed the MultiBac (Geneva Biotech, Indianapolis, IN, USA) system for protein expression
8 in insect cells (*Sf9*, Invitrogen) according to published protocols (29, 30). SARS-CoV-2 protein
9 complexes were purified using nickel-nitrilotriacetic acid affinity chromatography of the nsp8 N-terminal
10 8-histidine tag according to the manufacturer's specifications (Thermo Fisher Scientific, Waltham, MA,
11 USA). Purified protein was dialyzed into storage buffer (100 Tris-HCl (pH 8), 1000 mM NaCl, 5 mM
12 TCEP, 0.01 % Tween-20, 200 mM imidazole, and 40% glycerol), aliquoted and stored at -20 °C.

13

14 **Purification and recombinant protein expression of nsp13-helicase.**

15 The coding sequence for nsp13 from the SARS CoV-2 Washington isolate (Genbank
16 MN985325) was synthesized as an *E. coli* codon-optimized fragment (GenScript, Piscataway NJ) and
17 cloned into the *Bsal* site of the pSUMO plasmid (LifeSensors, Malvern, PA) to produce an N-terminal
18 six histidine-tagged SUMO-nsp13 fusion cassette (6XHis-SUMO-nsp13). Final plasmids were
19 sequence-verified through the UAMS Sequencing Core Facility using a 3130XL Genetic Analyzer
20 (Applied Biosystems, Foster City, CA). The SUMO-nsp13 construct was transformed into Rosetta2
21 cells, and colonies were grown overnight at 37°C in NZCYM (Research Products International, Mount
22 Prospect, IL) supplemented with kanamycin (50 µg/ml) and chloramphenicol (25 µg/ml). The cultures
23 were diluted 1:100 into fresh antibiotic-containing NZCYM media and grown to an OD_{600 nm} of 0.8-1.
24 The bacterial media was supplemented with 0.1 mM ZnSO₄ and 0.2% dextrose and cooled on ice for
25 10 min. Protein expression was induced with 0.2 mM isopropyl β-D-1-thiogalactopyranoside (IPTG) at
26 18°C for 12-16 hours. The cells were harvested by centrifugation at 4,000 x *g* for 15 min at 4°C, and
27 pellets stored at -80°C. All purifications steps were carried out on ice or at 4°C. Pellets were
28 resuspended in lysis buffer (50 mM sodium phosphate, pH 8.0, 300 mM NaCl, 1 mM β-mercaptoethanol,
29 10% glycerol and 20 mM imidazole) supplemented with 2 mM phenylmethylsulfonyl fluoride (PMSF)
30 and 1X EDTA-free protease inhibitor cocktail (Pierce). Bacteria were lysed by microfluidization and the
31 lysate clarified by centrifugation at 17,000 x *g* for 1 hour at 4°C. The His-tagged SUMO-nsp13 was
32 passed through a HisTrap FF column (Cytiva) equilibrated in lysis buffer at 1 ml/minute using a Cytiva
33 Akta FPLC. The affinity resin was washed with 20 column volumes of lysis buffer, and the protein eluted
34 with 10 column volumes of lysis buffer containing 200 mM imidazole. The pooled SUMO-nsp13-
35 containing fractions were dialyzed overnight into two changes of 20 mM imidazole-containing lysis
36 buffer, and the SUMO tag cleaved with ULP-1 for 4 hours at 4°C. Digestion was confirmed by SDS-
37 PAGE analysis. The His6-ULP-1 and His6-SUMO proteins were separated from the native nsp13 with
38 a second round of Ni²⁺-affinity chromatography as before. Nsp13-containing flow-thru fractions were
39 pooled, dialyzed overnight against two changes of low salt buffer (50 mM sodium phosphate, pH 6.8,

1 150 mM NaCl, 4 mM β -mercaptoethanol, 0.5 mM EDTA and 10% glycerol) and passed through a
2 HighTrap SP (Cytiva) cation exchange column. Under these conditions, nsp13 did not adhere to the SP
3 column and the flow-thru was collected in multiple fractions. The nsp13 was concentrated with an
4 Amicon Ultra-15 centrifugation filter unit to a volume of ~1.5 ml and loaded on to a Sephacyl S200-HR
5 HiPrep 26/60 column (Cytiva) equilibrated with nsp13 Storage Buffer (25 mM HEPES, pH 7.5, 150 mM
6 NaCl, 0.5 mM TCEP and 20% glycerol). The final nsp13 was quantified by UV spectrophotometry at
7 280 nm using the expected extinction coefficient of $68,785 \text{ M}^{-1} \text{ cm}^{-1}$ and confirmed using the BCA
8 Protein Assay (Pierce). Protein samples were aliquoted, flash frozen, and stored at -80°C .

9

10 **RNA hairpin fabrication.**

11 The fabrication of the RNA hairpin has been described in detail in (31). The RNA hairpin is
12 made of a 499 bp double stranded RNA stem terminated by a 20 nt loop that is assembled from three
13 ssRNA annealed together (**Figure S1A**). The RNA stem is flanked by two spacers, ~800 bp each,
14 containing a biotin- and a digoxigenin-handle, respectively. A gap of 25 nt between the biotin-handle
15 and the hairpin stem serves as the loading site for the polymerase (**Figure S1A**). At forces above 22
16 pN, the hairpin opens and frees up a 1043 nt ssRNA template for the SARS-CoV-2 polymerase (**Figure**
17 **S1B**). The RNA construct was synthesized by amplifying DNA fragments in PCR and *in vitro*
18 transcribing them (NEB HiScribe T7 High Yield RNA Synthesis Kit) after purification (Monarch PCR and
19 DNA cleanup kit). ssRNA fragments containing biotin- or digoxigenin-labels were synthesized with
20 biotin-UTP or digoxigenin-UTP (Jena Biosciences) in the reaction. Transcripts were mono-
21 phosphorylated (Antarctic Phosphatase and T4 Polynucleotide Kinase), annealed and ligated. The RNA
22 template sequence is provided in (26).

23

24 **Flow cell assembly and surface functionalization.**

25 The fabrication procedure for flow cells has been described in detail in (32). To summarize, we
26 sandwiched a double layer of Parafilm by two #1 coverslips, the top one having one hole at each end
27 serving as inlet and outlet, the bottom one being coated with a 0.1% m/V nitrocellulose dissolved in
28 amyl acetate solution. The flow cell is mounted into a custom-built holder and rinsed with ~1 ml of 1x
29 phosphate buffered saline (PBS) solution. 3 μm diameter polystyrene reference beads are attached to
30 the bottom coverslip surface by incubating 100 μL of a 1:1000 dilution in PBS (LB30, Sigma Aldrich,
31 stock conc.: 1.828×10^{11} particles per milliliter) for ~3 min. The tethering of the magnetic beads by the
32 RNA hairpin construct relies on a digoxigenin/anti-digoxigenin and biotin-streptavidin attachment at
33 the coverslip surface and the magnetic bead, respectively. Therefore, following a thorough rinsing of
34 the flow cell with PBS, 50 μL of anti-digoxigenin (50 mg/mL in PBS) is incubated for 30 min. The flow
35 cell was rinsed with 1 mL of 10 mM Tris, 1 mM EDTA pH 8.0, 750 mM NaCl, 2 mM sodium azide buffer
36 to remove excess of anti-digoxigenin followed by rinsing with another 0.5 ml of 1x TE buffer (10 mM
37 Tris, 1 mM EDTA pH 8.0 supplemented with 150 mM NaCl, 2 mM sodium azide). The surface is then
38 passivated by incubating bovine serum albumin (BSA, New England Biolabs, 10 mg/ml in PBS and 50%
39 glycerol) for 30 min and rinsed with 1x TE buffer.

1
2
3
4
5
6
7
8
9
10
11
12
13
14
15
16
17
18
19
20
21
22
23
24
25
26
27
28
29
30
31
32
33
34
35
36
37
38
39
40

Single-molecule SARS-CoV-2 primer-extension experiments.

20 μ L of streptavidin coated Dynabeads M-270 magnetic beads (ThermoFisher) were mixed with \sim 0.1 ng of RNA hairpin (total volume 40 μ L) and incubated for \sim 5 min before rinsing with \sim 2 ml of 1x TE buffer to remove any unbound RNA and the excess of magnetic beads. RNA tethers were sorted for functional hairpins by looking for the characteristic jump in extension of the correct length (\sim 0.6 μ m at 22 pN) due to the sudden opening of the hairpin during a force ramp experiment (**Figure S1C**) (26, 31). The flow cell was subsequently rinsed with 0.5 ml reaction buffer (50 mM HEPES pH 7.9, 10 mM DTT, 2 mM EDTA, 5 mM MgCl₂). After starting the data acquisition, the hairpin tether quality was tested by ramping the force up to monitor the typical cooperative opening signature of a hairpin, i.e. a vertical jump of the magnetic bead by \sim 0.6 μ m when reaching a critical opening force of \sim 22 pN (**Figure S1D**). The force was subsequently decreased to and maintained at 25 pN, unless specified otherwise. 100 μ L of reaction buffer containing the proteins and 500 μ M of {A,U,C,G}TP (Jena Biosciences) were flushed into the flow chamber (**Figure 1A**). SARS-CoV-2 core RTC activity traces were spotted as a downward movement of the bead, indicating the conversion of the ssRNA template into dsRNA, and therefore a shortening of the tether (**Figure 1A**). The recordings lasted 30 min. A temperature of 25 °C was maintained during all experiments. A custom written LabView routine controlled the data acquisition and the (x-, y-, z-) positions analysis/tracking of both the magnetic and reference beads (Sigma) in real-time (33). Mechanical drift correction was performed by subtracting the position of the reference bead from that of the magnetic beads, and further stabilized by an automated focusing routine that adaptively moves the objective to keep the reference bead at the same focal plane (26). The camera frame rate was fixed at 58 Hz.

Single-molecule experiments after pre-incubating proteins

For the experiments performed in **Figure 3A and S3**, 20 μ M of nsp12 (of either expression system) was added to 180 μ M of both nsp8 and nsp7. Next, the mixture was placed on a heating block at 25 °C for 4.5 hrs (nsp12-polymerase expressed in *E. coli*) or 6.5 hrs (nsp12-polymerase expressed in *Sf9*). After the specified waiting time, the proteins were diluted in reaction buffer to a final concentration of 0.2 μ M of nsp12-polymerase and 1.8 μ M of both nsp8 and nsp7. Finally, we proceeded by performing the primer-extension experiment as described above.

Single-molecule experiments after pre-incubating proteins with RNA.

After forming the RNA tethers as described above, proteins were added at specified concentration to the flow chamber. The recording was started. After 10 min we removed any excess of proteins in solution by rinsing the flow chamber with 500 μ L of reaction buffer. Finally, primer-extension experiments were performed after the system was complemented with the missing reagents (**Figures 3BC, S4-5**). In **Figures 3B, S4**, and **S5** the proteins were incubated together with 500 μ M of NTP to further confirm no activity can occur unless all nsps are present.

Data processing of RNA synthesis traces (elongation phase).

1 The change in extension in micron, resulting from the ssRNA to dsRNA conversion, was
2 subsequently converted into replicated nucleotides, low-pass filtered at 2 Hz and the dwell times were
3 extracted using a window of 10 nt as described in (11, 26, 34, 35). Elongation times and product lengths
4 were inferred from the final datapoint before the trajectory ended of the filtered traces (**Figure 4A**).
5 Product lengths shorter than the full length of the template were only considered if the bead stopped
6 moving downwards before the end of the recording. If the tether broke before the full product was
7 synthesized (seen as the loss of the bead), that event was excluded from both elongation time and
8 product length measurements.

9 10 **Data processing of activation times.**

11 When RNA extension could be observed in the trace, the activation time was taken as the time
12 between ending the addition of reagents into the flow chamber and the first datapoint when the bead
13 starts moving downwards (**Figure 1C**). Only tethers with an open hairpin before addition of the reagents
14 were considered (**Figure S1D**). Polymerase activity when the elongation phase started while still adding
15 reagents was clearly recognized (**Figure 1E**), but the start time/position of these events could not be
16 determined with high accuracy and these were assigned an activation time of zero seconds. Tethers
17 that remained until the end of the recording were considered to determine the fraction of tethers with
18 activity (**Figures S2, S7, and S8**). This showed that a considerable portion of traces showed no sign of
19 RNA extension during the 30 min recordings. Assuming that activation on different tethers are
20 independent, the activation efficiency results from a Bernoulli trial. The experimental estimate (η_A^{exp}) of
21 the primer-extension efficiency (η_A) is the total number of tethers on which we record activity (N_{rec}) over
22 to total number of quality RNA hairpin tethers (N_{HP})

$$\eta_A^{\text{exp}} = \frac{N_{\text{rec}}}{N_{\text{HP}}} \text{ and } \delta\eta_A^{\text{exp}} = \sqrt{\frac{\eta_A^{\text{exp}}(1-\eta_A^{\text{exp}})}{N_{\text{HP}}}} \quad (1).$$

23 We used that η_A^{exp} is an unbiased estimator of η_A , and plot the 95% confidence intervals ($\eta_A^{\text{exp}} \pm 2\delta\eta_A^{\text{exp}}$)
24 in **Figure S2**.

25 To extract the maximum likelihood estimator of the single-exponential time constant that best
26 describes the distribution of activation times we included events missed due to the limited experimental
27 time. This method has been described in detail in (36). Briefly, the maximum-likelihood estimator (MLE)
28 for the time constant in an single-exponential distribution would equal the average of all recorded times
29 (**Figure S2**),

$$\Delta t_A^{\text{rec}} = \frac{1}{N_{\text{rec}}} \sum_n^{N_{\text{rec}}} \Delta t_A^{(n)} \quad (2),$$

30 when there is no limit on the experimental observation time. In the above, $\Delta t_A^{(n)}$ corresponds to the
31 activation time recorded on the n^{th} out of the N_{rec} traces that initiate. With a finite experimental time
32 N_{cut} traces will not initiate within the experimental time T_{cut} , and the MLE that accounts for this is given
33 by

$$\Delta t_A^{\text{MLE}} = \Delta t_A^{\text{rec}} \left(1 + \frac{N_{\text{cut}} T_{\text{cut}}}{N_{\text{rec}} \Delta t_A^{\text{rec}}} \right) \quad (3).$$

1 To obtain an error estimate for Δt_A^{MLE} , 1000 bootstrap samples were drawn from the collection of $N_{\text{HP}} =$
 2 $N_{\text{rec}} + N_{\text{cut}}$ traces. In this manner we get a distribution of estimated activation times (**Equation 3**). The
 3 resulting 95% confidence intervals were used as the error estimates shown in **Figure 2**. In **Figures S7**
 4 **and S8** we overlay the distributions of recorded activation times with the exponential distribution with
 5 time constant **Equation 3** and total probability η_A^{exp} .

6
 7 The MLE of **Equation 3** was only applied to the experiments involving the individually purified
 8 nsps. At saturating concentrations of the purified complex, activation typically started before we stopped
 9 flushing reagents into the flow chamber (**Figure 1E** and **Figure 2E**). Yet, not all RNA tethers got
 10 converted into dsRNA during our recording (**Equation 1, Figure S2J**). The measured activation
 11 efficiencies (**Equation 1, Figure S2J**) showed little to no dependence on the concentration of the
 12 complex in this case, indicating that they do not originate in events missed due to our limited
 13 observational time; consequently we exclude these from our considerations. **Figure 2E** and **Figure S2I**
 14 therefore show the MLE of **Equation 2**. Error estimates are 95% confidence intervals from 1000
 15 bootstrap samples drawn from the N_{rec} recorded times.

16 17 **Modeling the activation time of the reconstituted core RTC.**

18 The reaction schema underlying our kinetic model is shown in **Figure S6**. We split the activation
 19 time into two parts; 1) a ‘slow’ process that includes the nsp7- and nsp8-dependent ‘activation step’
 20 (**Figures 5 and S6**), and 2) the time spent by the core RTC after being stabilized into an elongation-
 21 competent conformation, but before incorporation of the first nucleotide (**Figure S6**)

$$\Delta t_A^{\text{mod}} = \frac{1}{k_{\text{slow}}} + \frac{1}{k_{\text{fast}}^{\text{recon.}}} \quad (4)$$

22
 23 We will start by describing the rate-limiting transition (k_{slow}). Our results showed activation is orders of
 24 magnitudes faster in the presence of the RNA template (**Figures 3AB and S3**), hence we limit the
 25 activating conformational change to the RNA bound state. With this simplification the rate of the ‘slow’
 26 step in **Equation 4** equals the equilibrated fraction P_{bnd} of tethers with an assembled core RTC,
 27 multiplied by the intrinsic rate of undertaking the conformational change (k_{conf})

$$k_{\text{slow}} = k_{\text{conf}} \times P_{\text{bnd}} \quad (5).$$

29 Let c_7 , c_8 and c_{12} denote the concentrations of nsp7, nsp8 and nsp12-polymerase respectively. Given
 30 core RTC assembly and RNA binding happen before the rate limiting step, their respective probabilities
 31 of occurrence should be equilibrated, i.e. satisfy the law of mass action and detailed balance,

$$c_{\text{RTC}} = K_{\text{EQ}}^{\text{RTC}} c_7 c_8^2 c_{12} \quad (6),$$

$$P_{\text{bnd}} = K_{\text{EQ}}^{\text{bnd}} (1 - P_{\text{bnd}}) c_{\text{RTC}} \quad (7),$$

1
2 where P_{bnd} is the fraction of the RNA tethers with an assembled core RTCs bound to it. We also
3 introduced the equilibrium constants for assembling the core RTC ($K_{\text{EQ}}^{\text{RTC}}$) and binding the core RTC to
4 the RNA ($K_{\text{EQ}}^{\text{bnd}}$). The latter having a force-dependence as shown below. Given the large disparity in
5 apparent saturating concentrations using purified versus reconstituted core RTCs (**Figure 2**), we
6 assumed the total number of free nsps that complex remains small enough to not effect their
7 concentration in bulk, i.e. $K_{\text{EQ}}^{\text{RTC}} \ll K_{\text{EQ}}^{\text{bnd}}$. While losing some generality, we avoid allot of complexity in
8 the model. This allows us to use the model purely to focus on the effect of having a rate-limiting step
9 after equilibrated binding and assembly. Combining **Equations 5-7** yields

$$10 \quad k_{\text{slow}} = k_A \frac{c_7 c_8^2 c_{12} K_{\text{EQ}}^{\text{bnd}} K_{\text{EQ}}^{\text{RTC}}}{1 + c_7 c_8^2 c_{12} K_{\text{EQ}}^{\text{bnd}} K_{\text{EQ}}^{\text{RTC}}} \quad (8).$$

11
12 After rearranging the core RTC into an elongation-competent conformation, the protein complex can
13 still potentially unbind from the RNA before incorporating the first NTP (**Figure S6**). The above used
14 that this processes is much faster than the conformational change ($k_{\text{ub}} \gg k_{\text{conf}}$). However, this
15 assumption no longer holds true when competing with NTP incorporation (which occurs at $k_{\text{NTP}} \sim 70$
16 nt/s) (26). Instead of assuming equilibrium, we solve for the fraction of extended RNA molecules (P_{NTP})
17 from the flux-balances of RNA species after the core RTC changed conformation (**Figure S6**):

$$18 \quad \partial_t P_{\text{ub}} = -k_{\text{slow}} P_{\text{ub}}(t) + k_{\text{ub}} P_{\text{bnd}}(t) \quad (9),$$

$$19 \quad \partial_t P_{\text{bnd}} = +k_{\text{slow}} P_{\text{ub}}(t) - (k_{\text{ub}} + k_{\text{NTP}}) P_{\text{bnd}}(t) \quad (10),$$

$$20 \quad \partial_t P_{\text{NTP}} = k_{\text{NTP}} P_{\text{bnd}}(t) \quad (11).$$

21
22 Here, $P_{\text{ub}}(t)$ and $P_{\text{bnd}}(t)$ represent the time-dependent fractions of RNA molecules (not) bound by a
23 core RTC stabilized in its active conformation. The concentration of RNA molecules on the flow cell's
24 surface (picomolar range) is negligible when compared to the amount of protein available in solution. A
25 core RTC that unbinds from the RNA is therefore replaced by a different complex that must still undergo
26 the conformational change. Hence, the bare RNA enters the state of being occupied by an activated
27 core RTC at 'an effective binding rate' of k_{slow} (**Figure S6, Equations 10-11**). Incorporation of the first
28 nucleotide is treated as irreversible (**Figures 5 and S6**). Therefore, any additional number of RNA
29 molecules that are extended between times t and dt also equals the probability of having started NTP
30 incorporation within that time frame; the first-passage time distribution.

$$31 \quad \Psi_{\text{NTP}}^{\text{recon./purif.}}(t) = \partial_t P_{\text{NTP}}^{\text{recon./purif.}} \quad (12)$$

32

1 The superscripts 'recon./'purif.' are used to distinguish between the solutions to **Equations 9-11** under
 2 the initial conditions appropriate to the reconstituted/purified core RTC systems respectively. The
 3 reconstituted core RTC predominantly bound the RNA before changing conformation (**Figure 5 and**
 4 **Equation 5**, $P_{\text{bnd}}^{\text{recon.}}(t=0) = 1$, $P_{\text{ub}}^{\text{recon.}}(t=0) = P_{\text{NTP}}^{\text{recon.}}(t=0) = 0$). The inverse transition rate into the
 5 elongation phase equals the average first-passage time,
 6

$$\frac{1}{k_{\text{fast}}^{\text{recon.}}} = \int_0^{\infty} t \Psi_{\text{NTP}}^{\text{recon.}}(t) dt = \frac{1}{k_{\text{NTP}}} \left(1 + \frac{k_{\text{ub}}}{k_{\text{slow}}} \right) \quad (13)$$

7

8 **Modeling the activation time of the purified core RTC.**

9 Given a purified complex has already adopted the proper elongation-competent conformation,
 10 its activation time only includes the fast component,

$$\Delta t_A^{\text{mod}} = \frac{1}{k_{\text{fast}}^{\text{purif.}}} \quad (14)$$

11 Following the same strategy as done for $k_{\text{fast}}^{\text{recon.}}$, we once again determine the mean first passage time
 12 to incorporate the first nucleotide. Different from the case presented above, co-translated complexes in
 13 solution already are activated and thus rebind with an intrinsic binding rate (k_{bnd}). Assigning the same
 14 affinity of the purified and reconstituted RTC to the RNA (at a reference concentration of 1 μM), we
 15 invoke the law of mass action again,

$$k_{\text{bnd}} = K_{\text{EQ}}^{\text{bnd}} k_{\text{ub}} c_{\text{RTC}} \quad (15),$$

16

17 where we used $K_{\text{EQ}}^{\text{bnd}} \equiv k_{\text{bnd}}^{1 \mu\text{M}} / k_{\text{ub}}$; **Figure S6**. Replacing k_{slow} by k_{bnd} in **Equations 9-10**, results in the
 18 inverse reaction rate under the initial condition that the complex must first bind the RNA ($P_{\text{ub}}^{\text{purif.}}(t=0) =$
 19 1 , $P_{\text{bnd}}^{\text{purif.}}(t=0) = P_{\text{NTP}}^{\text{purif.}}(t=0) = 0$),

$$\frac{1}{k_{\text{fast}}^{\text{purif.}}} = \int_0^{\infty} t \Psi_{\text{NTP}}^{\text{purif.}}(t) dt = \frac{1}{k_{\text{bnd}}} \left(1 + \frac{k_{\text{ub}}}{k_{\text{NTP}}} \right) + \frac{1}{k_{\text{NTP}}} \quad (16).$$

20

21 **Incorporating force-dependent binding.**

22 At equilibrium, the fraction of bound complex follows the Boltzmann distribution

$$\frac{P_{\text{bnd}}}{1 - P_{\text{bnd}}} = e^{\frac{\Delta G_{\text{bnd}}}{k_{\text{B}} T}} \quad (17).$$

23 Here, we assigned a free-energy difference for binding the (assembled) RTC on the RNA (ΔG_{bnd}). The
 24 magnetic tweezers apply a constant force (F) to the template strand along the vertical direction (z -
 25 direction), thereby putting work into the system. Interactions with the template strand favor binding at
 26 lower force (**Figure 2F**), i.e. $\Delta G_{\text{bnd}}(F) \equiv \Delta G_{\text{bnd}}^0 + F \delta z$, with δz the length change induced to the RNA

1 by binding of the RTC. Defining a characteristic force of $F_0 = k_B T / \delta z$, **Equation 7** and **Equation 17**
 2 imply a force-dependent equilibrium constant,

3

$$K_{\text{EQ}}^{\text{bnd}}(F) \propto e^{-\frac{F}{F_0}} \quad (18).$$

4

5 **Equation 18** was applied in **Equation 13** and **Equation 16** to determine force-dependent activation
 6 times. The model parameter $K_{\text{EQ}}^{\text{bnd}} = k_{\text{bnd}}^{0 \text{ pN and } 1 \mu\text{M}} / k_{\text{ub}}$ is the constant of proportionality in **Equation 18**,
 7 denoting the equilibrium constant in the absence of an applied force. For notational convenience, the
 8 equations above still contain $K_{\text{EQ}}^{\text{bnd}}$, where the force-dependence (**Equation 18**) is implied.

9

10 **Fitting procedure using simulated annealing.**

11 The Simulated Annealing algorithm (37) is a commonly used algorithm for high-dimensional
 12 optimization problems. We used a custom-built Python code that has been more extensively described
 13 in (38). We optimized the loss-function (χ^2) with respect to our model parameters $\log_{10}(k_{\text{conf}}/1 \text{ s})$,
 14 $\log_{10}(K_{\text{EQ}}^{\text{RTC}}/1 \mu\text{M})$, $\log_{10}(K_{\text{EQ}}^{\text{bnd}}/(1 \mu\text{M})^3)$, $\log_{10}(k_{\text{ub}}/1 \text{ s})$, and $\log_{10}(F_0/1 \text{ pN})$. Model parameters have
 15 been transformed to make all fitted parameters lie within the same range.

16

$$\chi^2 = \sum_{i \in \left(\begin{smallmatrix} \text{all experiments} \\ \text{used for training} \end{smallmatrix} \right)} \frac{\left(\Delta t_A^{\text{mod},(i)} - \Delta t_A^{\text{exp},(i)} \right)^2}{\left(\delta t_A^{\text{exp},(i)} \right)^2} \quad (17).$$

17

18 That is, for every primer-extension experiment represented in **Figure 2**, we minimize the sum of
 19 differences of our model's predictions to the corresponding datapoint, weighted by the experimental
 20 error ($\delta t_A^{\text{exp},(i)}$) calculated as described above. Trial moves were generated by adding uniform noise of
 21 magnitude δ to the present value of each model parameter. The process was initiated with a noise
 22 strength of $\delta = 1.0$. In the initiation cycle, the temperature was adjusted until we had an acceptance
 23 fraction of 40-60% over 1000 trial moves, based on the Metropolis condition. After this initial cycle, the
 24 temperatures followed an exponential cooling scheme with a 1% cooling rate ($T_{k+1} = 0.99T_k$). At every
 25 temperature, we adjusted the noise strength δ until an acceptance fraction of 40-60% was reached over
 26 1000 trial moves. Once the desired acceptance fraction was reached, an additional 1000 trial moves
 27 were performed to allow the system to equilibrate before the next cooling step. Once the temperature
 28 had dropped to a factor 10^{-4} of its initial value, we applied the stop condition:

29

$$|\bar{\chi}_k^2 - \bar{\chi}_{k-1}^2| \leq 10^{-5} \bar{\chi}_{k-1}^2 \quad (2).$$

30

31 In the above, $\bar{\chi}_k^2$ denotes our cost function averaged over the last 1000 trial moves performed at
 32 temperature T_k . The optimization procedure was repeated 40 times (**Figure S9**). The parameter values
 33 with the lowest χ^2 were used to generate the curves shown in **Figure 2**.

34

1 Results

2 Slow activation by reconstituted SARS-CoV-2 core RTCs.

3 To determine the kinetics of the CoV polymerase complex during activation and elongation
4 phases, we built upon our previously developed single-molecule high-throughput magnetic tweezers
5 assay that monitors primer-extension of dozens of individual polymerases simultaneously (26, 34, 35,
6 39). Magnetic beads were tethered to the glass surface of a flow chamber by a 1043 nt single-stranded
7 (ss) RNA template that included a ~800 bp primer on the bead proximal side (31) (**Figure 1A** and **Figure**
8 **S1AB, Materials and Methods**). A pair of permanent magnets located above the flow chamber at a
9 fixed height applied a constant attractive force (25 pN, unless specified otherwise) to the magnetic
10 beads that stretched the RNA tethers (32, 40, 41). The three-dimensional position of each bead was
11 tracked in real-time, providing the extension of their respective tether (33). The RNA construct was
12 designed to form a ~500 bp hairpin when relaxed. The clear signature of the hairpin opening when
13 rapidly increasing the force was used to select for tethers with a properly presented primer (**Figure**
14 **S1CD**). During the elongation phase, the core RTC converted the ssRNA template into double-stranded
15 (ds) RNA, which decreased the extension of the tether (26).

16
17 Initial primer-extension assays were performed using a core RTC reconstituted from nsp7, nsp8
18 and nsp12-polymerase individually expressed and purified in *Escherichia coli* (*E. coli*) (**Figure 1B**,
19 **Materials and Methods**). We can define the activation time Δt_A as the time from injecting the core RTC
20 components and NTPs until the start of the elongation phase when the tether extension starts
21 decreasing (**Figure 1AC, Materials and Methods**). These single-molecule experiments showed that
22 the median activation time for the reconstituted core RTC (~5-10 min) greatly exceeded the elongation
23 time (~20-40 s) (**Figure 1CD**). To uncover the process(es) giving rise to the observed activation times,
24 we utilized a combination of different strategies to express and/or reconstitute the core RTC.

25
26 To perform primer-extension experiments with a core RTC expressed, processed and
27 assembled in the cell, we expressed the complex in *Sf9* cells from a bacmid encoding for nsp12-
28 polymerase, nsp8, nsp7, as well as nsp5-protease, and pulled down and purified the fully assembled
29 complex (hereafter: 'purified complex') (**Figure 1B, Materials and Methods**). Strikingly, the typical
30 activation time decreased to mere seconds when repeating the experiment using a comparable
31 concentration of purified complex (**Figure 1DE**). We note that all experiments in **Figure 1** were
32 performed at saturating concentrations of core RTC proteins (see below for discussion on **Figure 2**).

33
34 Given that individual nsps were expressed in *E. coli* and the purified complex was expressed
35 in *Sf9* cells (**Figure 1B**), we first evaluated whether the different expression system could promote the
36 purified complex' activation. To this end, we repeated our single-molecule experiments while
37 reconstituting the core RTC with an nsp12-polymerase expressed in *Sf9* cells (**Figure 1BF, Materials**
38 **and Methods**). The resulting reconstituted core RTC, with nsp12-polymerase expressed in insect cells,
39 did not activate rapidly (**Figure 1DF**). We concluded that the difference in expression systems cannot

1 account for most of the observed differences in activation times between bacteria- and insect-derived
2 polymerases.

3

4 **Assembly and RNA binding of the core RTC cannot account for the observed activation times.**

5 As opposed to the purified complex, the individual proteins of the reconstituted core RTC must
6 come together to assemble into a complex. We questioned whether the time required to assemble the
7 reconstituted core RTC can explain its slower activation as has been suggested in literature (23, 24).
8 To this end, we performed primer-extensions under varying concentrations of one of the three nsp,
9 while keeping the other two unchanged. Here, we used the nsp12-polymerase expressed in *E. coli* to
10 reconstitute the core RTC. While the average activation times measured responded to the varying
11 protein concentrations, we noticed a stronger effect on the fraction of RNA primer-templates that got
12 extended during our 30 min recording (**Figure S2**). This indicated a significant and varying proportion
13 of events (up to ~75% at the lowest nsp concentrations) were missed as they took longer than the
14 duration of our experiment. The estimated (effective) activation times shown in **Figure 2A-D,F** are
15 maximum likelihood estimates accounting for the fraction of events that exceed the observation time
16 (**Materials and Methods**).

17

18 Elongation started sooner on average at higher concentrations of nsp7, with average activation
19 times dropping by ~4 fold over the tested concentration range (**Figure 2A**). However, at saturating nsp7
20 concentrations (above 1.8 μM), a substantial effective activation time of ~1000 s remained (**Figure 2A**),
21 i.e. still significantly slower than the purified complex (**Figure 1E**). A similar trend was seen when
22 increasing either the nsp8 or nsp12-polymerase concentration (**Figure 2BC**), i.e. the activation time
23 decreased until an average time of ~1000 s remained at saturation, meaning for concentrations of
24 $\text{nsp8} \geq 1.8 \mu\text{M}$ and $\text{nsp12-polymerase} \geq 0.2 \mu\text{M}$. The remaining time can therefore not be explained by
25 the need to bring the complex together.

26

27 To evaluate whether the time required to find and bind the RNA accounts for the remaining
28 activation time, we fixed the stoichiometry (nsp12:nsp7:nsp8 of 1:9:9) and varied the overall
29 concentration both with nsp12-polymerase expressed in bacterial and insect cells (**Figure 2D**). In both
30 cases, an effective activation time of ~1000 s remained, even above saturating proteins concentration,
31 showing that this time is both independent of host-specific post-translational modifications on the nsp12-
32 polymerase and core RTC assembly, but must be intrinsic to the core RTC components. On the other
33 hand, when we varied the concentration of the purified complex, an activation time of mere seconds
34 was reached at saturation, i.e. activity was detected while flushing in reaction buffer with all proteins
35 into the flow chamber (**Figure 1E** and **Figure 2E**). The saturating concentration of the purified complex
36 is in the tens of nanomolar range (**Figure 2E**), while hundreds of nanomolar of the reconstituted core
37 RTC were required to saturate activity (**Figure 2D**). As the purified complex only needs to find the
38 primer, a lower saturation concentration suggests that the affinity of the complex to the RNA is much
39 greater than that of the proteins to themselves (at the stoichiometry used).

40

1 The force applied by the magnetic tweezers provides an additional gauge of the affinity of the
2 core RTC for the primer-template. Namely, elevated tension in the template strand (above ~35 pN)
3 destabilizes the primer-template junction, hindering a proper placement of the terminal base in the
4 polymerase's active site upon binding (26). Furthermore, applying tension probes possible
5 conformational changes of core RTC along the direction of the force (e.g. the upstream RNA contacts
6 made by the nsp8 tails (18, 20)), and any conformational change orthogonal to the direction of the force
7 remains unaffected. While we observe a steep increase in effective activation time at forces beyond 40
8 pN, the effective activation time remains ~1000 s at lower forces (**Figure 2F**). Taken together, neither
9 the time needed to assemble the core RTC nor the time spent on binding to the RNA can fully account
10 for the observed activation times. We thus conclude that another process must take place to enable the
11 reconstituted core RTC to enter the elongation phase.

12 13 **A slow conformational change renders the core RTC elongation-competent.**

14 As the duration of the activation phase still greatly exceeded that of the elongation phase at
15 lower forces (**Figure 2F**), we reasoned that the remaining time should be accounted for by processes
16 other than direct interactions along the template RNA. If a slow conformational change is to occur after
17 the core RTC assembled, providing sufficient time for the nsps to interact should induce rapid activation
18 upon introduction of the nucleotides. We pre-incubated nsp12-polymerase with nsp7 and nsp8 for over
19 four hours prior to conducting the single-molecule primer extension assay (**Figure 3A**). To counteract
20 any loss of active proteins during incubation, proteins were added together at 100-fold the concentration
21 used in the flow chamber during the experiment (**Materials and Methods**). Rapid activation was indeed
22 observed with pre-incubated nsp7, nsp8 and nsp12-polymerase individually expressed in *E. coli*
23 (**Figure 3A**). Given sufficient time, reconstituted core RTCs can show the same phenotypical short
24 activation times as the purified complex. However, in experiments performed without any pre-incubation
25 up to ~80% of core RTCs are capable of activating within 600 s (**Figure S2**). Incubating the nsps for 10
26 min (nsp12-polymerase expressed in *E. coli*) did not result in any rapidly activating core RTCs (**Figure**
27 **S3**). The core RTC reconstituted with nsp12-polymerase expressed in *Sf9* did not show rapid activation
28 even after incubation with the co-factors for over 6.5 hours (**Figure 3A**). If the purified complex only
29 activated rapidly because the proteins resided together in the same cell for hours, what then allowed
30 the reconstituted core RTCs to activate within 10 min during our experiments? We surmised that access
31 to the template RNA may have aided the reconstituted system. Introducing the nsps to the RNA in the
32 flow chamber for 10 min indeed resulted in rapid activation upon addition of nucleotides (82% of events
33 using nsp12-polymerase expressed in *E. coli*; 95% of events using nsp12-polymerase expressed in
34 *Sf9*) (**Figure 3B, Materials and Methods**). Taken together, independent of the expression system, pre-
35 incubating the nsps with the RNA reproduced the rapid activation observed with the purified complex
36 (**Figure 3B**). The activation time of ~1000 s that remained at saturating protein concentrations (**Figure**
37 **2A-D**) can thus be accounted for by a process that took place during the incubation with the RNA
38 (**Figure 3AB**). Given the majority of this time is neither spent on assembling the core RTC nor binding
39 the RNA, we concluded that the core RTC must undergo a conformational change that renders it
40 elongation-competent. While the protein complex, at least in part, rearranges itself orthogonally to the

1 RNA template (**Figure 2F**), interactions with the template RNA greatly stabilize the elongation-
2 competent conformation (**Figure 3B**).

3

4 **The conformational change enabling elongation requires both nsp7 and nsp8**

5 Having established the existence and necessity of a conformational change for RNA synthesis
6 activity, we next questioned whether nsp7 and nsp8 facilitate it. If the co-factors are a necessary
7 condition, allowing only nsp12-polymerase to access the RNA for 10 min should not result in the rapid
8 activation as seen in the experiments represented in **Figure 3B**. As expected, adding nsp12-
9 polymerase alone with NTP to the RNA did not result in any activity (**Figure 3C**). We subsequently
10 removed all free-floating proteins and thereafter injected the reaction buffer containing nsp7, nsp8 and
11 NTP (**Materials and Methods**). The newly added co-factors can only form a core RTC if a nsp12-
12 polymerase is still bound to an RNA template after rinsing the flow chamber. We successfully recovered
13 activity, but only after approximately 10 min (**Figure 3C**). The nsp12-polymerase preincubated with the
14 RNA template was not yet elongation-competent, but required co-factors to enact the needed
15 conformational change.

16

17 To establish whether both nsp7 and nsp8 are needed to induce the conformational change we
18 repeated the experiment described in **Figure 3C**, though this time we added one of the two co-factors
19 together with nsp12-polymerase during pre-incubation with the RNA in the flow chamber (**Figure S4**).
20 Not only are both co-factors required to activate the core RTC, as no activity was recorded after
21 incubation despite the presence of NTP (**Figure S4**), initially omitting one of them severely lowered or
22 even abolished the primer-extension activity. Namely, nsp12-polymerase incubated with nsp7 and the
23 RNA template could only rarely be activated through addition of new nsp7 and nsp8 (~5% activity vs
24 ~50% activity when incubating the three proteins with the RNA). Moreover, in the rare cases of
25 activation observed (4 events in total, ~80 tethers surviving the full duration of the measurement) it was
26 only after an activation time of more than an hour (**Figure S4A**). Allowing nsp12-polymerase and nsp8
27 to preincubate with the RNA template completely blocked the RTC from activation (**Figure S4B**). No
28 activity was observed within an hour from the point at which all nsps were present (**Figure S4B**). These
29 results suggest nsp12-polymerase explores a conformation space, only to be locked into a stable
30 conformer by the co-factors nsp7 and nsp8. When only one of the two co-factors is available, the
31 polymerase appears to adopt a conformation that prevents RNA synthesis. Escaping this state requires
32 significantly more time (**Figure S4**).

33

34 **The elongation-competent conformation of the core RTC is stable for several hours, but is** 35 **reversed upon loss of nsp7 and nsp8**

36 To establish if a core RTC stably resides in its active conformer, we pre-incubated the purified
37 complex for over eight hours in reaction buffer and at room temperature before performing primer-
38 extensions (**Materials and Methods**). We still observed rapid activation on ~25% of all tethers upon
39 NTP addition (**Figure S5**), indicating that a substantial fraction of the complexes were still elongation-
40 competent. To test if some of the tethers showed no activity due to disassembly of a bound core RTC,

1 we waited for an additional 10 min, rinsed the flow chamber, and introduced new nsp7, nsp8 and NTP
2 in an attempt to rescue any nsp12-polymerase bound without co-factor (**Figure S5**). Re-introduction of
3 new nsp7 and nsp8 led to new activity (**Figure S5**). Together with the reduction in saturating
4 concentration for the purified complex (i.e. pre-assembled) discussed above, **Figure 2DE**), these
5 results indicate that nsp12-polymerase binds the RNA template with a higher affinity than nsp7 and
6 nsp8 bind to nsp12-polymerase. A long-lasting activation phase was observed again, indicating that the
7 core RTC reverts to its inactive form upon losing co-factors (**Figure S5**).

8
9 Taken together, the core RTC must undergo a conformational change to initiate RNA synthesis
10 (**Figure 3AB**). This conformational change requires both nsp7 and nsp8 to be present during the
11 assembly process to prevent the complex from being stabilized in an inactive form (**Figure 3C** and
12 **Figure S4**). After successfully having undergone the correct transition, the core RTC is stably locked
13 into an active conformation for several hours (**Figure S5**).

14 **Dynamics during the elongation phase are independent of those during the activation phase.**

15
16 Next, we set out to determine whether the long lag-times prior to detectible primer-extension in
17 bulk (23, 24) are completely explained by the time required to escape the activation phase. To this end,
18 we examined the dynamics during the ensuing elongation phase. Our single-molecule experiments
19 allow us to directly tell if an increased yield of product RNA is due to more core RTCs successfully
20 entering the elongation phase, or due to an enhanced rate of RNA synthesis. During the elongation
21 phase, the tethered magnetic bead moved downwards (**Figure 1AC**). Converting the height drop to the
22 fraction of ssRNA that has been converted into dsRNA gives rise to the position of the core RTC along
23 the template (34) (**Figure 4A**). Comparing the purified complex and reconstituted core RTCs, we
24 observed no discernible difference amongst their time trajectories (**Figure 4A**). Given the rich,
25 stochastic, variation amongst traces within an experiment we quantified the duration of the elongation
26 phase (Δt_E) together with the resulting length of the product (ΔL_E) (**Figure 4AB**). No significant
27 difference in either quantity was detected amongst the three expression systems tested (**Figure 4B**).
28 To completely characterize the dynamics of the obtained time traces we further extracted the distribution
29 of times required to add ten consecutive nucleotides (11, 26, 35, 39, 42). None of the three dwell time
30 distributions shown in **Figure 4C** were significantly different from the distribution we previously reported
31 to hold true for a (reconstituted) core RTC (26). The pause-free elongation rate can be estimated by the
32 location of the main peak seen in the histograms (26), and the three of them coincide in **Figure 4C**. We
33 found no evidence for any influence of the choice of expression system on the core RTC's dynamics
34 during the elongation phase. As the activation times increased with decreasing co-factor
35 concentration(s) (**Figure 2AB**), we examined the elongation phases under varying nsp7 (**Figure 4D-F**)
36 or nsp8 (**Figure 4G-I**) concentrations. The concentration of co-factors in solution had no influence on
37 elongation times, product lengths, or the dwell time distributions. All measured distributions coincide
38 with our previously reported one (11, 26).

39

1 We conclude that any lag-time before RNA production seen in bulk biochemistry experiments
2 (23, 24) stems entirely from altered dynamics during the activation phase. Our previous model of the
3 elongation phase in the reconstituted system (26) should therefore hold true irrespective of the dynamics
4 of the activation phase.

5 6 **Activation of the core RTC follows its equilibrated assembly**

7 To further test if the existence of a conformational change after core RTC assembly can
8 quantitatively describe our data we built a kinetic model based on our above findings. **Figure 5** shows
9 the predominant assembly and activation pathway of the core RTC towards processive RNA synthesis.
10 The complete reaction pathway underlying the kinetic model fitted to the data is shown in **Figure S6**
11 **(Materials and Methods)**. The core RTC is able to sequentially assemble on the RNA, starting with
12 nsp12-polymerase, followed by the addition of nsp7 and nsp8 (**Figure 3C** and **Figure S5**). Both co-
13 factors (nsp7 and nsp8) must be present to obtain active core RTCs to any appreciable degree (**Figure**
14 **S4**). Furthermore, the core RTC activates within minutes in the presence of RNA, whereas the apo
15 form, i.e. without RNA, requires several hours of incubating the nsps to see rapid activation (**Figure**
16 **3AB** and **Figure 5**).

17
18 We observed long activation times of several minutes, even at saturating protein concentrations
19 (**Figure 2A-D**), indicating that activation occurs after assembly of the core RTC onto the RNA, which in
20 itself can be treated as equilibrated within that timespan (**Figure 5** and **Figure S6**). For each
21 experiment, the distribution of activation times was consistent with a single exponential with a
22 characteristic timescale dependent on protein concentrations (**Figure S7**) and force (**Figure S8**).
23 Hence, we conclude that a single rate-limiting conformational change is responsible for the activation
24 of the core RTC (indicated with the rate k_{conf} in **Figure 5** and **Figure S6**). The purified complex showed
25 rapid elongation upon addition into the flow chamber (**Figure 1E**), suggesting this complex had already
26 gone through activation, likely during protein expression. Furthermore, the activated conformation of
27 the core RTC proved to be reasonably stable for over 8 hours of pre-incubation (**Figure S5**). We
28 therefore modelled the activation step as irreversible (**Figure 5**, **Figure S6**). Having adopted the
29 elongation-competent conformation, the activation time is only limited by the rate of nucleotide
30 incorporation ($k_{\text{NTP}} \sim 70 \frac{\text{nt}}{\text{s}}$ at 25 °C, **Figure 4**) (26). It took micromolars of (co-)factors (**Figure 2A-C**,
31 **Figure S2C-F**), while just tens of nanomolar of the purified complex was needed to saturate activity
32 (**Figure 2E** and **Figure S2I-J**). Furthermore, activity can be restored on RNA initially bound by nsp12-
33 polymerase alone by adding new nsp7 and nsp8 (**Figure 3C** and **Figure S5**). Hence, we assume that
34 the core RTC binds much tighter to the RNA than the complex is held together (**Figure S6**, **Materials**
35 **and Methods**). The kinetic model that we fitted to the data globally (**Figure S6**, **Figure 2**, **Materials**
36 **and Methods**) quantitatively captures all experiments in a unified manner (**Figure S9** shows the
37 distribution of fit parameters with fit results within 1% of the best fit, **Materials and Methods**). Although
38 the model allows for multiple cycles of core RTCs binding and activating prior to starting RNA synthesis
39 (**Figure S6**, **Materials and Methods**), we find a good agreement with our data when the unbinding rate
40 (k_{ub}^{-1} between 1 – 20 s, **Figure S9**) is much lower than the rate of nucleotide addition (70 s^{-1} , $k_{\text{NTP}}^{-1} \ll$

1 k_{ub}^{-1}). Taken together, following equilibrated assembly ($K_{\text{EQ}}^{\text{RTC}}$ between $0.06 - 0.99 \mu\text{M}^{-4}$, **Figure S9**) and
2 RNA binding ($K_{\text{EQ}}^{\text{bnd}}$ between $60 - 980 \mu\text{M}^{-1}$ at 25 pN, with a characteristic force F_0 between $7.6 - 8.2$
3 pN, **Figure S9**), the rate of starting RNA synthesis is truly limited by the time required for the first core
4 RTC to undergo the conformational change (k_{conf}^{-1} between $773 - 800$ s, **Figure S9**).

5

6 **SARS-CoV-2 core RTC activation remains slow in the presence of nsp13-helicase.**

7 During a viral infection, the core RTC associates with additional nsps to form an extended RTC,
8 such as nsp13-helicase (15, 43). We addressed whether the associated with nsp13-helicase to the core
9 RTC results in a similarly large barrier towards elongation-competence. We performed primer-extension
10 experiments with the three core RTC proteins at saturating concentrations ($0.2 \mu\text{M}$ nsp12-polymerase,
11 $1.8 \mu\text{M}$ nsp7, and $1.8 \mu\text{M}$ nsp8), as well as purified nsp13-helicase at the indicated concentration
12 (**Figure S10AB, and Materials and Methods**). Structural studies have reported that two nsp13-
13 helicases bind the core RTC, one of them also binding the template RNA (15). Accordingly, we see a
14 reduction in activation times upon addition of nsp13-helicase (**Figure S10C-E**). While an increase in
15 tension lowered the affinity of the core RTC to the RNA (**Figure 2F**), addition of nsp13-helicase
16 increased its affinity. We further note that in the presence of saturating amounts of nsp13-helicase, i.e.
17 above 10 nM, the duration of the activation phase is still set by one characteristic timescale (**Figure**
18 **S10C**). Moreover, the addition of nsp13-helicases only minimally increased the success rate of the
19 primer-extension reaction (**Figure S10F**). In terms of our kinetic model, the helicase increases both the
20 RNA-binding affinity ($K_{\text{EQ}}^{\text{bnd}}$) and transition rate into elongation-competency (k_{conf}). Regardless, an
21 average activation time of ~ 360 s remains at a saturating concentration of 20 nM nsp13-helicase
22 (**Figure S10C-E**). This demonstrates that the time needed for a conformational change identified for
23 the core RTC remains relevant when viewed in the context of the extended complex.

24

25 **Discussion**

26 The coronavirus RTC, in particular the 'core RTC', fulfills the essential role of replicating the
27 viral genome (13) and is therefore a key target for antiviral drugs. There is a wealth of structural (8, 10,
28 18, 20) and biochemical studies focused on understanding and inhibiting the CoV polymerase's RNA
29 synthesis capabilities (9, 11, 12, 26, 28, 44). The assembly of the core RTC was earlier proposed to be
30 the rate-limiting step in the RNA synthesis reaction (23, 24). The present study reveals that an already
31 assembled core RTC must undergo a conformational change that represents the true rate-limiting step
32 towards processive elongation.

33

34 We expanded the single-molecule high-throughput magnetic tweezers assay we previously
35 developed (26) to assess the lag time between injection of the RTC proteins into the flow chamber
36 and the start of RNA synthesis (**Figure 1A**). We investigated how varying the stoichiometry and
37 concentration of the core RTC proteins, as well as their mode of expression, impacted both activation
38 and elongation phases. We showed that the approximately ten minutes activation time (**Figure 1**) did
39 not result from either the time required for the core RTC to assemble or to bind the RNA (**Figure 2**), but
40 rather from a conformational change within the complex (**Figures 3, Figure 5**).

1
2
3
4
5
6
7
8
9
10
11
12
13
14
15
16
17
18
19
20
21
22
23
24
25
26
27
28
29
30
31
32
33
34
35
36
37
38
39
40

We note that when expressing nsp12-polymerase in *E. coli*, the gene sequence was codon optimized not for total protein production but to maximize activity in bulk (27, 45) (**Materials and Methods**). Rare codons were intentionally maintained within the coding sequence with the idea of retaining natural pause sites for the ribosome to allow the protein more time to fold into a functional conformer during translation. While clearly not an elongation-competent conformer from the onset (**Figure 1C**), an altered free-energy landscape for folding the nsp12-polymerase can facilitate access to the elongation-competent conformer. This likely explains why pre-incubating the *E. coli* expressed nsp12-polymerase with nsp7 and nsp8 resulted in rapid activation, while repeating the same experiment with the *Sf9* expressed nsp12-polymerase whose coding sequence was codon-optimized for protein yield, i.e. lacking the rare codons, did not (**Figure 3A**). It also supports our hypothesis that nsp7 and nsp8 stabilize a conformation in which nsp12-polymerase properly exposes its active site to the RNA template.

Activation of the SARS-CoV-2 core RTC requires the co-factors nsp7 and nsp8 (**Figure 3, Figure 5**). Cryogenic-electron microscopy (cryo-EM) studies of apo-core RTC and RNA bound core RTC revealed nsp8 must undergo a large conformational change allowing its N-terminal tails to form rigid contacts ~28 bp upstream of the active site (18–20). While this is clearly a conformational change required for RNA synthesis, our data does not support the interpretation that the rotation of the nsp8s constitutes the activation step. Namely, using a purified core RTC or pre-incubating the individual nsp8s allowed for rapid activation (**Figure 1D, Figure 3B**). In these core RTCs, the nsp8 monomers must still unfold their N-terminal tails prior to starting RNA synthesis (17, 19). Given the nsp8 tails align along the RNA, establishing the contacts should be tension-dependent. Furthermore, we saw a reduction in the mean activation time when including nsp13-helicase (**Figure S10**), suggesting that nsp13-helicase successfully bound the extended nsp8-tails (15). Finally, varying the tension applied to the template RNA did not reduce the (effective) activation time to seconds (**Figure 2F**). Therefore, the activation step we reveal here is a distinct conformational change that, at least in part, rearranges protein domains that either do not interact with the RNA or move orthogonal to the force. We hypothesize that the conformational change is mainly in nsp12-polymerase, with the co-factors stabilizing a conformer in which the RNA is positioned properly for RNA synthesis. In the absence of either nsp7 or nsp8, nsp12-polymerase is forced into a conformation that is inactive and is harder to escape from (**Figure S4**).

Previous studies have identified viral genomic RNA-polymerase interactions to initiate either replication or transcription in RNA viruses. The dengue virus polymerase (NS5) interacts with the stem loop 5 in the viral genome, which enables its transition into an ‘elongation complex’ (46). Alphaviruses have a promotor sequence in their genome that activates the RdRp to transcribe a subgenomic RNA encoding for structural proteins (47). Our results also indicate an important role for the RNA in activating the core RTC, which was orders of magnitudes faster with RNA as opposed to without (**Figure 3**). The rich structure of the SARS-CoV-2 genome (48) may contain a motif yet to be discovered to recruit and activate the RTC.

1
2
3
4
5
6
7
8
9
10
11
12
13
14
15
16
17
18
19
20
21
22
23
24
25
26
27
28
29
30
31
32
33
34
35
36
37
38
39
40

Recent studies demonstrated that a P323L mutation in the nsp12-polymerase, present in most SARS-CoV-2 variants of concern (49), increases the core RTC's primer-extension rate (50) and the viruses' fitness (51). The mutated residue stabilizes the nsp12/nsp8 interface (50). Based on our results, we suspect the mutation modulates the RTC's activation time. One may speculate how such a mutation could be beneficial to the virus. Seminal work on CoV murine hepatitis virus showed that stopping translation in infected cells rapidly resulted in a drop of (-)RNA synthesis (52), indicating that a continuous production of nsps was necessary for viral RNA synthesis during infection. Hence, the virus is seemingly assembling and activating new RTCs throughout the infectious cycle. During a viral infection, the extended RTC incorporates additional components beyond the core. These include nsp13-helicases (15), an nsp10-nsp14 complex with exonuclease and methyltransferase activities (16, 53), which may also associate with nsp16 (54), and the capping co-factor nsp9 (27), among others (16). The experiments of **Figure S10** show that the polymerase-helicase complex must still undergo a post-assembly conformational change to become elongation-competent. The extended activation time of the core RTC may enable the recruitment of all essential nsps before replication begins. The association of additional components could influence the kinetics of this activation, a possibility that warrants future investigations.

Our results provide a mechanistic insight into the assembly and activation of the core RTC, establishing a platform to recruit other nsps and assemble a complete and functional CoV RTC to reveal the molecular determinants of CoV replication.

Acknowledgements

We thank Gonzalo Cosa for fruitful discussions. DD was supported by the Interdisciplinary Center for Clinical Research (IZKF) at the University Hospital of the University of Erlangen-Nuremberg, the German Research Foundation grant DFG-DU-1872/4-1, BaSyC – Building a Synthetic Cell™ Gravitation grant (024.003.019) of the Netherlands Ministry of Education, Culture and Science (OCW) and the Netherlands Organisation for Scientific Research (NWO), NIH fundings R01 AI161841-01, U19 AI171292 and U19 AI171421, and NWO funding OCENW.XL21.XL21.115. IA was supported by NIH funding R01 GM067153. KDR was supported by NIGMS funding R35-GM12260.

Author contributions

DD, SCB, AD, MK, CEC, JJA designed the research. AD, SCB and MK performed the experiments, as well as processed and analyzed the data. MK and MD developed the kinetic model. BW and IA provided recombinant nsp12-polymerase expressed in *E. coli*. TKA and RNK provided recombinant nsp12-polymerase expressed in *Sf9*, as well as nsp7 and nsp8. DK, HWL and MG provided co-translated core RTC. JCM and KDR provided recombinant nsp13-helicase. DD supervised the research. MK and DD wrote the article. All the authors edited the article.

Competing interests

1 The authors declare that they have no competing interests.

2

3 **Data availability**

4 Data will be made publically available upon publication (DOI link will be added).

5

6 **References**

7

- 8 1. Beigel, J.H., Tomashek, K.M., Dodd, L.E., Mehta, A.K., Zingman, B.S., Kalil, A.C., Hohmann, E.,
9 Chu, H.Y., Luetkemeyer, A., Kline, S., *et al.* (2020) Remdesivir for the Treatment of
10 Covid-19 — Final Report. *N Engl J Med*, **383**, 1813–1826.

- 11 2. Jayk Bernal, A., Gomes Da Silva, M.M., Musungaie, D.B., Kovalchuk, E., Gonzalez, A., Delos
12 Reyes, V., Martín-Quirós, A., Caraco, Y., Williams-Diaz, A., Brown, M.L., *et al.* (2022)
13 Molnupiravir for Oral Treatment of Covid-19 in Nonhospitalized Patients. *N Engl J*
14 *Med*, **386**, 509–520.

- 15 3. Sanderson, T., Hisner, R., Donovan-Banfield, I., Hartman, H., Løchen, A., Peacock, T.P. and
16 Ruis, C. (2023) A molnupiravir-associated mutational signature in global SARS-CoV-2
17 genomes. *Nature*, **623**, 594–600.

- 18 4. Martinot, M., Jary, A., Fafi-Kremer, S., Leducq, V., Delagreverie, H., Garnier, M., Pacanowski, J.,
19 Mékinian, A., Pirenne, F., Tiberghien, P., *et al.* (2021) Emerging RNA-Dependent RNA
20 Polymerase Mutation in a Remdesivir-Treated B-cell Immunodeficient Patient With
21 Protracted Coronavirus Disease 2019. *Clinical Infectious Diseases*, **73**, e1762–e1765.

- 22 5. Stevens, L.J., Pruijssers, A.J., Lee, H.W., Gordon, C.J., Tchesnokov, E.P., Gribble, J., George, A.S.,
23 Hughes, T.M., Lu, X., Li, J., *et al.* (2022) Mutations in the SARS-CoV-2 RNA-dependent
24 RNA polymerase confer resistance to remdesivir by distinct mechanisms. *Sci Transl*
25 *Med*, **14**, eabo0718.

- 26 6. Chien, M., Anderson, T.K., Jockusch, S., Tao, C., Li, X., Kumar, S., Russo, J.J., Kirchdoerfer, R.N.
27 and Ju, J. (2020) Nucleotide Analogues as Inhibitors of SARS-CoV-2 Polymerase, a Key
28 Drug Target for COVID-19. *J. Proteome Res.*, **19**, 4690–4697.

- 1 7. Chinthapatla,R., Sotoudegan,M., Srivastava,P., Anderson,T.K., Moustafa,I.M., Passow,K.T.,
2 Kennelly,S.A., Moorthy,R., Dulin,D., Feng,J.Y., *et al.* (2023) Interfering with nucleotide
3 excision by the coronavirus 3'-to-5' exoribonuclease. *Nucleic Acids Research*, **51**, 315–
4 336.
- 5 8. Feng,J.Y., Du Pont,V., Babusis,D., Gordon,C.J., Tchesnokov,E.P., Perry,J.K., Duong,V.,
6 Vijapurapu,A., Zhao,X., Chan,J., *et al.* (2022) The Nucleoside/Nucleotide Analogs
7 Tenofovir and Emtricitabine Are Inactive against SARS-CoV-2. *Molecules*, **27**, 4212.
- 8 9. Gordon,C.J., Tchesnokov,E.P., Feng,J.Y., Porter,D.P. and Götte,M. (2020) The antiviral
9 compound remdesivir potently inhibits RNA-dependent RNA polymerase from
10 Middle East respiratory syndrome coronavirus. *Journal of Biological Chemistry*, **295**,
11 4773–4779.
- 12 10. Malone,B.F., Perry,J.K., Olinares,P.D.B., Lee,H.W., Chen,J., Appleby,T.C., Feng,J.Y.,
13 Bilello,J.P., Ng,H., Sotiris,J., *et al.* (2023) Structural basis for substrate selection by the
14 SARS-CoV-2 replicase. *Nature*, **614**, 781–787.
- 15 11. Seifert,M., Bera,S.C., van Nies,P., Kirchdoerfer,R.N., Shannon,A., Le,T.-T.-N., Meng,X.,
16 Xia,H., Wood,J.M., Harris,L.D., *et al.* (2021) Inhibition of SARS-CoV-2 polymerase by
17 nucleotide analogs from a single-molecule perspective. *eLife*, **10**, e70968.
- 18 12. Tchesnokov,E.P., Gordon,C.J., Woolner,E., Kocinkova,D., Perry,J.K., Feng,J.Y., Porter,D.P.
19 and Götte,M. (2020) Template-dependent inhibition of coronavirus RNA-dependent
20 RNA polymerase by remdesivir reveals a second mechanism of action. *Journal of*
21 *Biological Chemistry*, **295**, 16156–16165.
- 22 13. Steiner,S., Kratzel,A., Barut,G.T., Lang,R.M., Aguiar Moreira,E., Thomann,L., Kelly,J.N. and
23 Thiel,V. (2024) SARS-CoV-2 biology and host interactions. *Nat Rev Microbiol*,
24 10.1038/s41579-023-01003-z.
- 25 14. Narwal,M., Armache,J.-P., Edwards,T.J. and Murakami,K.S. (2023) SARS-CoV-2 polyprotein
26 substrate regulates the stepwise Mpro cleavage reaction. *Journal of Biological*
27 *Chemistry*, **299**, 104697.

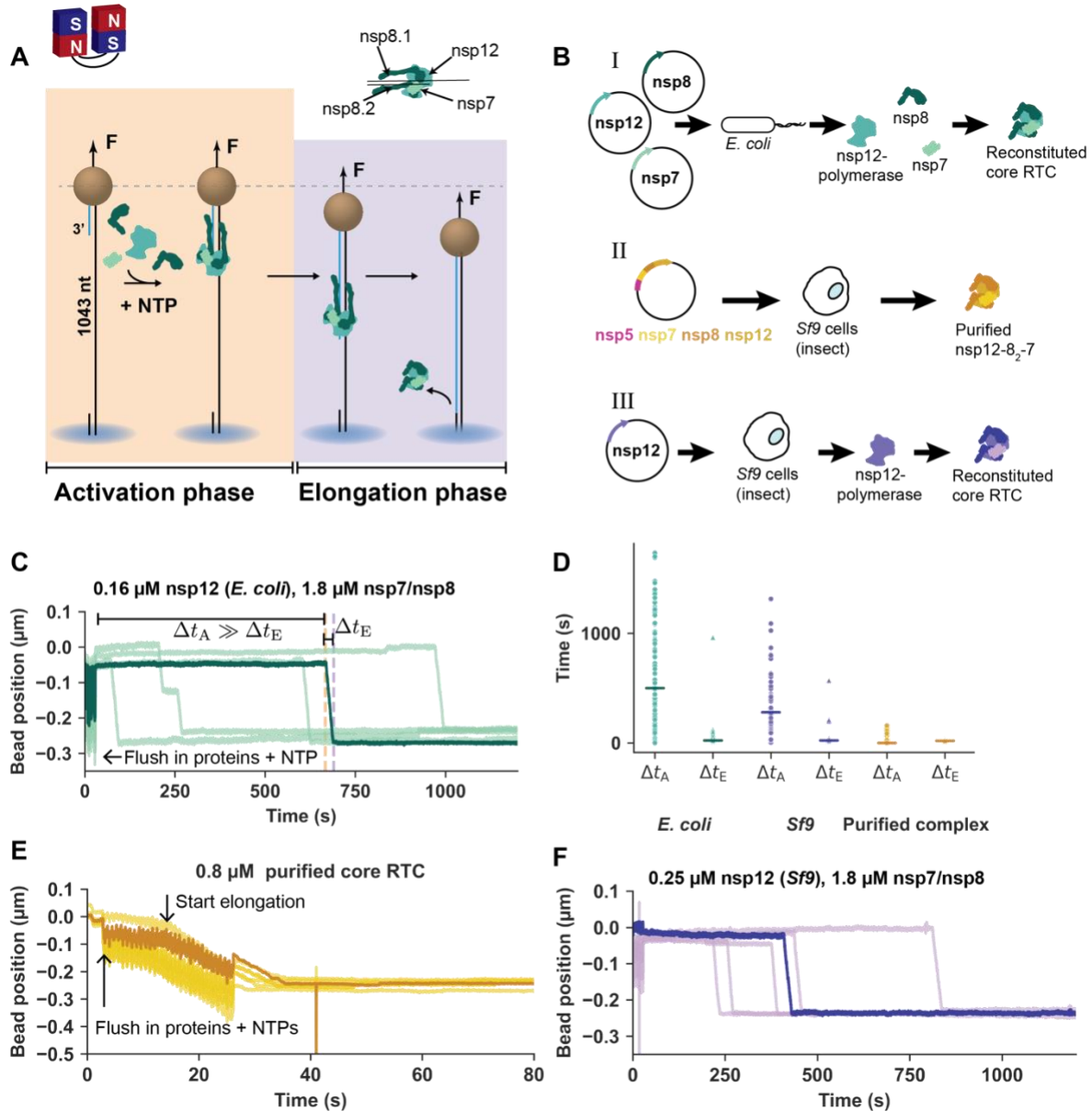
- 1 15. Chen,J., Malone,B., Llewellyn,E., Grasso,M., Shelton,P.M.M., Olinares,P.D.B., Maruthi,K.,
2 Eng,E.T., Vatandaslar,H., Chait,B.T., *et al.* (2020) Structural Basis for Helicase-
3 Polymerase Coupling in the SARS-CoV-2 Replication-Transcription Complex. *Cell*, **182**,
4 1560-1573.e13.
- 5 16. Yan,L., Yang,Y., Li,M., Zhang,Y., Zheng,L., Ge,J., Huang,Y.C., Liu,Z., Wang,T., Gao,S., *et al.*
6 (2021) Coupling of N7-methyltransferase and 3'-5' exoribonuclease with SARS-CoV-2
7 polymerase reveals mechanisms for capping and proofreading. *Cell*, **184**, 3474-
8 3485.e11.
- 9 17. Gao,Y., Yan,L., Huang,Y., Liu,F., Zhao,Y., Cao,L., Wang,T., Sun,Q., Ming,Z., Zhang,L., *et al.*
10 (2020) Structure of the RNA-dependent RNA polymerase from COVID-19 virus.
11 *Science*, **368**, 779–782.
- 12 18. Hillen,H.S., Kokic,G., Farnung,L., Dienemann,C., Tegunov,D. and Cramer,P. (2020)
13 Structure of replicating SARS-CoV-2 polymerase. *Nature*, **584**, 154–156.
- 14 19. Kirchdoerfer,R.N. and Ward,A.B. (2019) Structure of the SARS-CoV nsp12 polymerase
15 bound to nsp7 and nsp8 co-factors. *Nat Commun*, **10**, 2342.
- 16 20. Wang,Q., Wu,J., Wang,H., Gao,Y., Liu,Q., Mu,A., Ji,W., Yan,L., Zhu,Y., Zhu,C., *et al.* (2020)
17 Structural Basis for RNA Replication by the SARS-CoV-2 Polymerase. *Cell*, **182**, 417-
18 428.e13.
- 19 21. Anderson,T.K., Hoferle,P.J., Chojnacki,K.J., Lee,K.W., Coon,J.J. and Kirchdoerfer,R.N. (2024)
20 An alphacoronavirus polymerase structure reveals conserved replication factor
21 functions. *Nucleic Acids Research*, **52**, 5975–5986.
- 22 22. Biswal,M., Diggs,S., Xu,D., Khudaverdyan,N., Lu,J., Fang,J., Blaha,G., Hai,R. and Song,J.
23 (2021) Two conserved oligomer interfaces of NSP7 and NSP8 underpin the dynamic
24 assembly of SARS-CoV-2 RdRP. *Nucleic Acids Research*, **49**, 5956–5966.
- 25 23. Campagnola,G., Govindarajan,V., Pelletier,A., Canard,B. and Peersen,O.B. (2022) The
26 SARS-CoV nsp12 Polymerase Active Site Is Tuned for Large-Genome Replication. *J*
27 *Virology*, **96**, e0067122.

- 1 24. Subissi,L., Posthuma,C.C., Collet,A., Zevenhoven-Dobbe,J.C., Gorbalenya,A.E., Decroly,E.,
2 Snijder,E.J., Canard,B. and Imbert,I. (2014) One severe acute respiratory syndrome
3 coronavirus protein complex integrates processive RNA polymerase and exonuclease
4 activities. *Proc Natl Acad Sci U S A*, **111**, E3900–E3909.
- 5 25. Wilamowski,M., Hammel,M., Leite,W., Zhang,Q., Kim,Y., Weiss,K.L., Jedrzejczak,R.,
6 Rosenberg,D.J., Fan,Y., Wower,J., *et al.* (2021) Transient and stabilized complexes of
7 Nsp7, Nsp8, and Nsp12 in SARS-CoV-2 replication. *Biophysical Journal*, **120**, 3152–
8 3165.
- 9 26. Bera,S.C., Seifert,M., Kirchdoerfer,R.N., van Nies,P., Wubulikasimu,Y., Quack,S., Papini,F.S.,
10 Arnold,J.J., Canard,B., Cameron,C.E., *et al.* (2021) The nucleotide addition cycle of the
11 SARS-CoV-2 polymerase. *Cell Reports*, **36**, 109650.
- 12 27. Wang,B., Svetlov,V., Wolf,Y.I., Koonin,E.V., Nudler,E. and Artsimovitch,I. (2021) Allosteric
13 Activation of SARS-CoV-2 RNA-Dependent RNA Polymerase by Remdesivir
14 Triphosphate and Other Phosphorylated Nucleotides. *mBio*, **12**,
15 10.1128/mbio.01423-21.
- 16 28. Gordon,C.J., Lee,H.W., Tchesnokov,E.P., Perry,J.K., Feng,J.Y., Bilello,J.P., Porter,D.P. and
17 Götte,M. (2022) Efficient incorporation and template-dependent polymerase
18 inhibition are major determinants for the broad-spectrum antiviral activity of
19 remdesivir. *J Biol Chem*, **298**, 101529.
- 20 29. Berger,I., Fitzgerald,D.J. and Richmond,T.J. (2004) Baculovirus expression system for
21 heterologous multiprotein complexes. *Nat Biotechnol*, **22**, 1583–1587.
- 22 30. Bieniossek,C., Richmond,T.J. and Berger,I. (2008) MultiBac: Multigene Baculovirus-Based
23 Eukaryotic Protein Complex Production. *Current Protocols in Protein Science*, **51**,
24 5.20.1-5.20.26.
- 25 31. Papini,F.S., Seifert,M. and Dulin,D. (2019) High-yield fabrication of DNA and RNA
26 constructs for single molecule force and torque spectroscopy experiments. *Nucleic
27 Acids Research*, **47**, e144–e144.

- 1 32. Quack,S. and Dulin,D. (2024) Surface Functionalization, Nucleic Acid Tether
2 Characterization, and Force Calibration for a Magnetic Tweezers Assay. *Methods Mol*
3 *Biol*, **2694**, 403–420.
- 4 33. Cnossen,J.P., Dulin,D. and Dekker,N.H. (2014) An optimized software framework for real-
5 time, high-throughput tracking of spherical beads. *Review of Scientific Instruments*,
6 **85**, 103712.
- 7 34. Dulin,D., Vilfan,I.D., Berghuis,B.A., Hage,S., Bamford,D.H., Poranen,M.M., Depken,M. and
8 Dekker,N.H. (2015) Elongation-Competent Pauses Govern the Fidelity of a Viral RNA-
9 Dependent RNA Polymerase. *Cell Reports*, **10**, 983–992.
- 10 35. Dulin,D., Arnold,J.J., van Laar,T., Oh,H.-S., Lee,C., Perkins,A.L., Harki,D.A., Depken,M.,
11 Cameron,C.E. and Dekker,N.H. (2017) Signatures of Nucleotide Analog Incorporation
12 by an RNA-Dependent RNA Polymerase Revealed Using High-Throughput Magnetic
13 Tweezers. *Cell Reports*, **21**, 1063–1076.
- 14 36. Eslami-Mosallam,B., Katechis,I. and Depken,M. (2019) Fitting in the Age of Single-
15 Molecule Experiments: A Guide to Maximum-Likelihood Estimation and Its
16 Advantages. In Joo,C., Rueda,D. (eds), *Biophysics of RNA-Protein Interactions*,
17 Biological and Medical Physics, Biomedical Engineering. Springer New York, New
18 York, NY, pp. 85–105.
- 19 37. Kirkpatrick,S., Gelatt,C.D. and Vecchi,M.P. (1983) Optimization by Simulated Annealing.
20 *Science*, **220**, 671–680.
- 21 38. Eslami-Mossallam,B., Klein,M., Smagt,C.V.D., Sanden,K.V.D., Jones,S.K., Hawkins,J.A.,
22 Finkelstein,I.J. and Depken,M. (2022) A kinetic model predicts SpCas9 activity,
23 improves off-target classification, and reveals the physical basis of targeting fidelity.
24 *Nat Commun*, **13**, 1367.
- 25 39. Dulin,D., Berghuis,B.A., Depken,M. and Dekker,N.H. (2015) Untangling reaction pathways
26 through modern approaches to high-throughput single-molecule force-spectroscopy
27 experiments. *Current Opinion in Structural Biology*, **34**, 116–122.

- 1 40. Dulin,D. (2024) An Introduction to Magnetic Tweezers. In Heller,I., Dulin,D.,
2 Peterman,E.J.G. (eds), *Single Molecule Analysis : Methods and Protocols*, Methods in
3 Molecular Biology. Springer US, New York, NY, pp. 375–401.
- 4 41. Ostrofet,E., Papini,F.S. and Dulin,D. (2018) Correction-free force calibration for magnetic
5 tweezers experiments. *Sci Rep*, **8**, 15920.
- 6 42. Dulin,D., Vilfan,I.D., Berghuis,B.A., Poranen,M.M., Depken,M. and Dekker,N.H. (2015)
7 Backtracking behavior in viral RNA-dependent RNA polymerase provides the basis for
8 a second initiation site. *Nucleic Acids Res*, 10.1093/nar/gkv1098.
- 9 43. Yan,L., Zhang,Y., Ge,J., Zheng,L., Gao,Y., Wang,T., Jia,Z., Wang,H., Huang,Y., Li,M., *et al.*
10 (2020) Architecture of a SARS-CoV-2 mini replication and transcription complex. *Nat*
11 *Commun*, **11**, 5874.
- 12 44. Maheden,K., Todd,B., Gordon,C.J., Tchesnokov,E.P. and Götte,M. (2021) Inhibition of viral
13 RNA-dependent RNA polymerases with clinically relevant nucleotide analogs.
14 *Enzymes*, **49**, 315–354.
- 15 45. Wang,B., Svetlov,V., Nudler,E. and Artsimovitch,I. (2021) Lost in translation: codon
16 optimization inactivates SARS-CoV-2 RdRp. 10.1101/2021.01.24.428004.
- 17 46. Osawa,T., Aoki,M., Ehara,H. and Sekine,S. (2023) Structures of dengue virus RNA
18 replicase complexes. *Molecular Cell*, **83**, 2781-2791.e4.
- 19 47. Strauss,J.H. and Strauss,E.G. (1994) The alphaviruses: gene expression, replication, and
20 evolution. *Microbiological Reviews*, **58**, 491–562.
- 21 48. Cao,C., Cai,Z., Xiao,X., Rao,J., Chen,J., Hu,N., Yang,M., Xing,X., Wang,Y., Li,M., *et al.* (2021)
22 The architecture of the SARS-CoV-2 RNA genome inside virion. *Nat Commun*, **12**,
23 3917.
- 24 49. Kim,S.-M., Kim,E.-H., Casel,M.A.B., Kim,Y.-I., Sun,R., Kwak,M.-J., Yoo,J.-S., Yu,M., Yu,K.-M.,
25 Jang,S.-G., *et al.* (2023) SARS-CoV-2 variants with NSP12 P323L/G671S mutations
26 display enhanced virus replication in ferret upper airways and higher transmissibility.
27 *Cell Reports*, **42**, 113077.

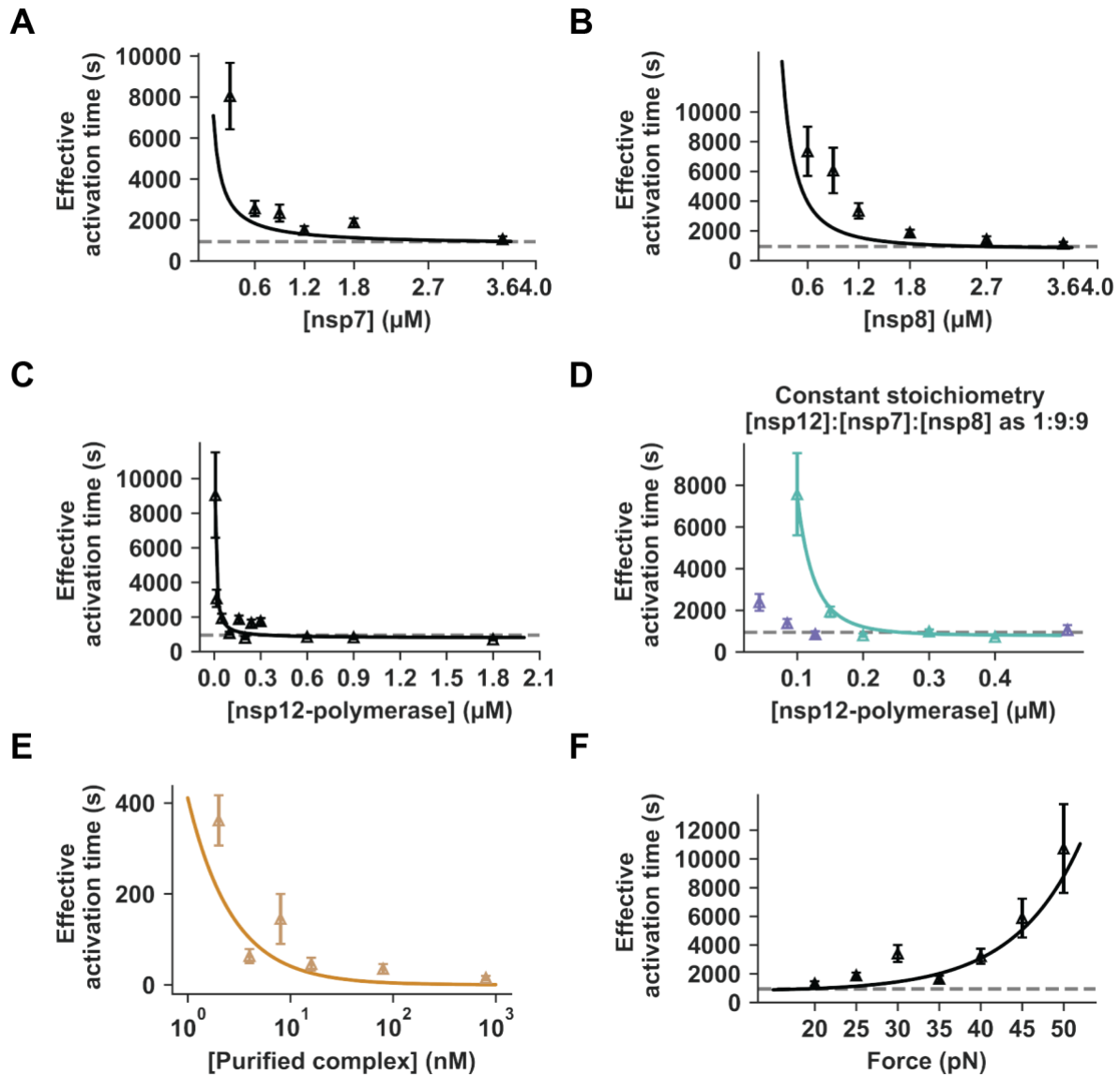
- 1 50. Ferrer-Orta,C., Vázquez-Monteagudo,S., Ferrero,D.S., Martínez-González,B., Perales,C.,
2 Domingo,E. and Verdaguer,N. (2024) Point mutations at specific sites of the nsp12–
3 nsp8 interface dramatically affect the RNA polymerization activity of SARS-CoV-2.
4 *Proceedings of the National Academy of Sciences*, **121**, e2317977121.
- 5 51. Goldswain,H., Dong,X., Penrice-Randal,R., Alruwaili,M., Shawli,G.T., Prince,T.,
6 Williamson,M.K., Raghwani,J., Randle,N., Jones,B., *et al.* (2023) The P323L
7 substitution in the SARS-CoV-2 polymerase (NSP12) confers a selective advantage
8 during infection. *Genome Biology*, **24**, 47.
- 9 52. Sawicki,S.G. and Sawicki,D.L. (1986) Coronavirus minus-strand RNA synthesis and effect
10 of cycloheximide on coronavirus RNA synthesis. *J Virol*, **57**, 328–334.
- 11 53. Moeller,N.H., Shi,K., Demir,Ö., Belica,C., Banerjee,S., Yin,L., Durfee,C., Amaro,R.E. and
12 Aihara,H. (2022) Structure and dynamics of SARS-CoV-2 proofreading
13 exoribonuclease ExoN. *Proc. Natl. Acad. Sci. U.S.A.*, **119**, e2106379119.
- 14 54. Matsuda,A., Plewka,J., Rawski,M., Mourão,A., Zajko,W., Siebenmorgen,T., Kresik,L., Lis,K.,
15 Jones,A.N., Pachota,M., *et al.* (2024) Despite the odds: formation of the SARS-CoV-2
16 methylation complex. *Nucleic Acids Research*, 10.1093/nar/gkae165.
- 17



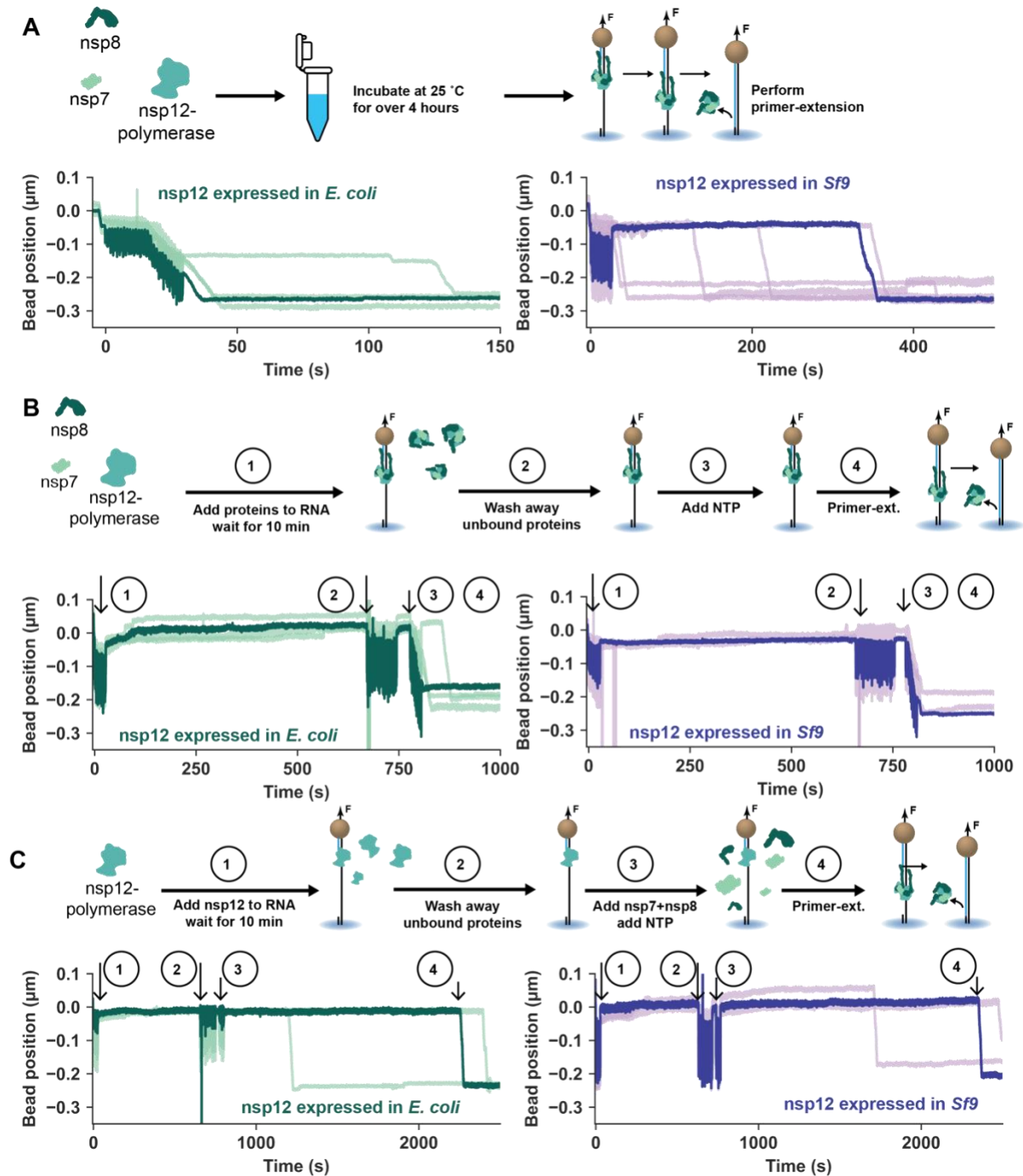
1

2 **Figure 1: Slow activation by reconstituted SARS-CoV-2 core RTCs. (A)** Schematic of the magnetic
 3 tweezers assay to monitor activation and elongation by the SARS-CoV-2 core RTC (**Materials and**
 4 **Methods**). **(B)** Schematic representation different methods of obtaining the core RTC used throughout
 5 this work. (I) nsp7, nsp8 and nsp12-polymerase were separately and recombinantly expressed in *E.*
 6 *coli*, (II) purification of core RTC complex after expressing a bacmid containing nsp5-Mpro (main
 7 protease), nsp8, nsp7, and nsp12-polymerase in *Sf9* cells, (III) nsp7, nsp8 and nsp12-polymerase were
 8 separately and recombinantly expressed in *E. coli* and nsp12-polymerase was recombinantly
 9 expressed in *Sf9* (**Materials and Methods**). Color coding for the different core RTCs is kept in
 10 subsequent figures to represent to related data. **(C)** Example time traces for the reconstituted SARS-
 11 CoV-2 core RTC using 0.16 μM nsp12-polymerase (see (I) in panel B) and 1.8 μM of nsp7 and nsp8.
 12 The orange and purple dashed lines indicate the end of the activation and elongation phases. Δt_A and
 13 Δt_E are their respective durations. **(D)** Δt_A and Δt_E for all recorded traces in experiments of which
 14 representative subsets are shown in panels C, E and F. Horizontal markers indicate the group medians.

- 1 **(E)** Example time traces using 0.8 μM of the purified SARS-CoV-2 core RTC (see (II) in panel B). **(F)**
- 2 Example time traces for the reconstituted SARS-CoV-2 core RTC using 0.25 μM nsp12-polymerase
- 3 expressed in *Sf9* (see (III) in panel B) and 1.8 μM of nsp7 and nsp8.
- 4



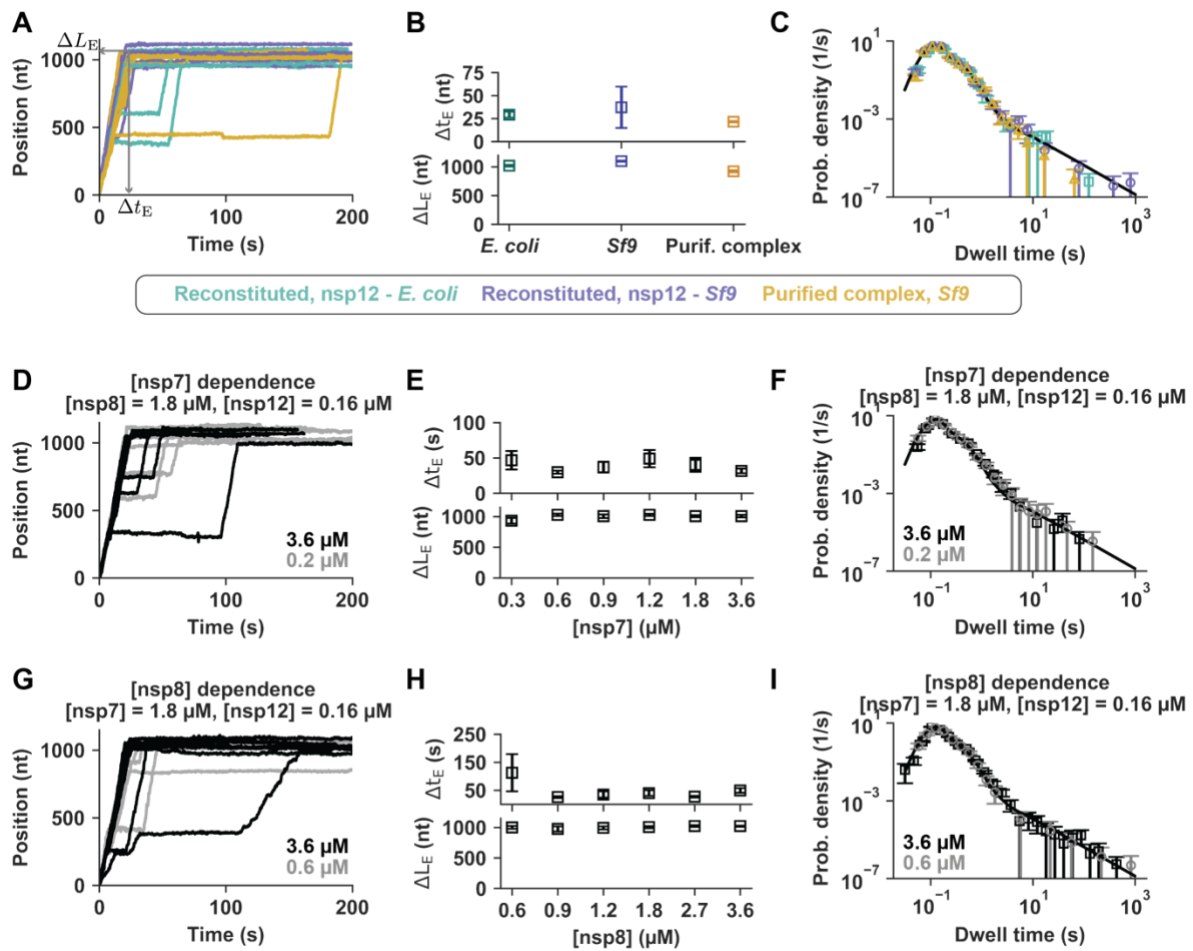
1
 2 **Figure 2: Assembly and RNA binding of the core RTC cannot fully account for the observed**
 3 **activation times.** When not being varied, experiments were performed using 0.16 μM of nsp12-
 4 polymerase, 1.8 μM nsp7, 1.8 μM nsp8, and 25 pN. Effective activation times across **(A)** nsp7
 5 concentration, **(B)** nsp8 concentration, **(C)** nsp12-polymerase concentration (expressed in *E. coli*). **(D)**
 6 Activation times versus nsp12-polymerase concentration, while maintaining a constant stoichiometry of
 7 [nsp12-polymerase]:[nsp7]:[nsp8] as 1:9:9 in solution. Core RTC reconstituted using nsp12-polymerase
 8 expressed in *E. coli* (turquoise) or *Sf9* (purple). **(E)** Activation times versus concentration of purified
 9 complex. **(F)** Activation times versus force (reconstituted core RTC, all proteins expressed in *E. coli*).
 10 Error bars represent 95% confidence intervals estimated through bootstrapping (**Materials and**
 11 **Methods**). Effective activation times shown incorporate the fraction of events lasting longer than the
 12 recording (**Materials and Methods**). Solid curves are the best fit of our mechanochemical model
 13 (**Materials and Methods, Figure 5 and Figure S6**). Dashed horizontal lines are shown to guide-the-
 14 eye.



1

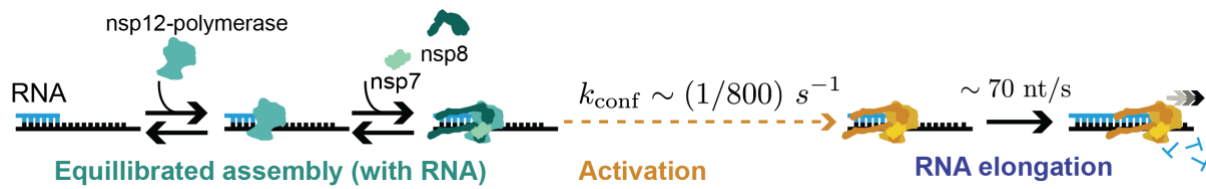
2 **Figure 3: Presence of the template RNA reduces activation times.** Example time traces are shown
 3 for a reconstituted core RTC. **(A)** Nsps were added together 4.5 hrs (nsp12-polymerase expressed in
 4 *E. coli*) or 6.5 hrs (nsp12-polymerase expressed in *Sf9*) prior to diluting them to 0.2 μM nsp12, 1.8 μM
 5 nsp7 and nsp8 and performing primer-extensions. **(B)** (1) The proteins were added to the RNA tethering
 6 the magnetic beads in the flow chamber. (2) Ten minutes later 500 μL of reaction buffer was used to
 7 rinse the flow chamber from free-floating proteins. (3) Finally, ribonucleotides were added and (4)
 8 Activation typically started during step (3). **(C)** (1) After tethering the magnetic beads to the RNA, 0.2
 9 μM of nsp12-polymerase and 500 μM of NTP were added. (2) Ten minutes later 500 μL of reaction

- 1 buffer was used to remove free-floating proteins. (3) The nucleotides were reintroduced together with
- 2 1.8 μ M of nsp7 and nsp8. (4) RTC elongation activity.
- 3



1
2 **Figure 4: The activation phase and the mode of core RTC proteins expression do not influence**
3 **the kinetics of the elongating core RTC. (A)** Example time traces during elongation phase of either
4 reconstituted core RTC with 0.16 μM nsp12-polymerase expressed in *E. coli*, and 1.8 μM nsp7 and
5 nsp8 (turquoise), reconstituted core RTC with 0.2 μM nsp12-polymerase expressed in *Sf9* and 1.8 μM
6 nsp7 and nsp8 (purple), or 2 nM of co-translated core RTC (yellow). **(B)** Mean elongation times (Δt_E)
7 and product lengths (ΔL_E), and **(C)** dwell time distributions for the entire set of activity traces recorded.
8 The solid line in panel C represents the distribution we previously reported in Ref. (26). **(D)** Example
9 time traces during elongation phase of a reconstituted core RTC (nsp12-polymerase expressed in *E.*
10 *coli*) at 1.8 μM (black) and 0.2 μM (grey) of nsp7. **(E)** Mean elongation times and product lengths, and
11 **(F)** dwell time distributions across nsp7 concentrations. **(G)** Example time traces during elongation of
12 reconstituted core RTC (nsp12-polymerase expressed in *E. coli*) at 1.8 μM (black) and 0.6 μM (grey)
13 of nsp8. **(H)** Mean elongation times and product lengths, and **(I)** dwell time distribution across nsp8
14 concentrations. All error bars represent 95% confidence intervals determined as described in **Materials**
15 **and Methods.**

16



1

2

3

4

5

Figure 5: The activation of the core RTC into a processive polymerase is rate-limited by a slow conformational change following assembly. Nsp12-polymerase rapidly binds to the RNA and thereafter recruits the co-factors nsp7 and nsp8, followed by a slow and irreversible conformational change that activates the core RTC into processive elongation.